

AMERICAN UNIVERSITY OF BEIRUT

DYNAMIC MODELING OF A HYBRID AUTONOMOUS
UNDERWATER VEHICLE WITH EFFICIENT THREE
DIMENSIONAL PATH PLANNING METHODS

by
BILAL I. WEHBE

A thesis
submitted in partial fulfillment of the requirements
for the degree of Master of Engineering
to the Department of Mechanical Engineering
of the Faculty of Engineering and Architecture
at the American University of Beirut

Beirut, Lebanon
May 7 2014

AMERICAN UNIVERSITY OF BEIRUT

DYNAMIC MODELING OF A HYBRID AUTONOMOUS
UNDERWATER VEHICLE WITH EFFICIENT THREE
DIMENSIONAL PATH PLANNING METHODS

by
BILAL I. WEHBE

Approved by:



Dr. Elie Shammas, Assistant Professor
Mechanical Engineering
Advisor



Dr. Daniel Asmar, Assistant Professor
Mechanical Engineering
Co-Advisor



Dr. Joseph Zeaiter, Assistant Professor
Chemical Engineering
Member of Committee

Date of thesis defense: May 7 2014

AMERICAN UNIVERSITY OF BEIRUT

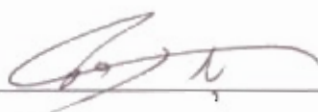
THESIS, DISSERTATION, PROJECT RELEASE FORM

Student Name: Wahbe Bilal Issam
Last First Middle

Master's Thesis Master's Project Doctoral Dissertation

I authorize the American University of Beirut to: (a) reproduce hard or electronic copies of my thesis, dissertation, or project; (b) include such copies in the archives and digital repositories of the University; and (c) make freely available such copies to third parties for research or educational purposes.

I authorize the American University of Beirut, **three years after the date of submitting my thesis, dissertation, or project**, to: (a) reproduce hard or electronic copies of it; (b) include such copies in the archives and digital repositories of the University; and (c) make freely available such copies to third parties for research or educational purposes.



Signature

15-May-14

Date

This form is signed when submitting the thesis, dissertation, or project to the University Libraries

ACKNOWLEDGEMENTS

I would like to express my deep gratitude for some people whom without their support this thesis would have been much harder to accomplish.

I would like to first thank my advisor Dr. Elie Shammas, whom I'm deeply indebted to, for his great support and wise coaching throughout my stay at AUB. He had a big influence on me since he continuously motivated and helped me develop an eager spirit of a researcher. I am very grateful that I got the chance to work with such a humble, intelligent, and knowledgeable person.

I would like to thank my second advisor Dr. Daniel Asmar for his tremendous guidance and support, he has such a brilliant mind and spirit. I admit that this work would have not been possible without his persistent help and constructive criticism.

In addition, a special thanks to my committee member Dr. Joseph Zeaiter for his generous and supportive efforts that helped make this project a reality.

I also like to thank the Lebanese National Council for Scientific Research (LNCSR) for funding this project.

I am deeply grateful for my friends and colleagues at the lab and in the faculty for their confidence and support.

Special thanks goes to my family for always being there, to my great brothers and parents who without their support I wouldn't be where I am today.

Thank you

AN ABSTRACT OF THE THESIS OF

Bilal I. Wehbe for Master of Engineering
Major: Mechanical Engineering

Title: Dynamic Modeling of a Hybrid Autonomous Underwater Vehicle with Efficient Three Dimensional Path Planning Methods

This thesis presents the design of a hybrid autonomous underwater vehicle (HAUV), which combines the features of a propelled vehicle and those of an underwater glider. The mechanical design is briefly introduced, describing the main structure and specifications of the vehicle. We demonstrate its dynamic model and describe several simulations to showcase its locomotive capabilities. Sliding mode control techniques are implemented to control the heading and steering velocities. Results show the successful servoing of the vehicle under various modes. The main contribution of this work is in the proposed motion planning technique to solve for trajectories from a start to a goal configuration. Our method generates feasible trajectories by integrating two planar Dubins curves. In fact, the motion planning technique is devised to not only generate feasible trajectories but also to assess their optimality.

CONTENTS

ACKNOWLEDGEMENTS	v
ABSTRACT	vi
LIST OF FIGURES	ix
LIST OF TABLES	x
1 INTRODUCTION	1
1.1 Thesis Contribution	3
1.2 Thesis Outline	4
2 MECHANICAL DESIGN	5
2.1 Design Concept	5
2.2 Design Features	7
2.2.1 Wings	7
2.2.2 Pressure Shaft Sealing	8
2.2.3 Adapters and Sealing	8
2.2.4 Other Components	9
3 MODELING SIMULATION AND CONTROL	11
3.1 System Modeling	11
3.1.1 Coordinate Frames and Transformations	11
3.1.2 Rigid Body Dynamics	12
3.1.3 Hydrodynamic Forces and Moments	13
3.1.3.1 Added Mass	13
3.1.3.2 Hydrodynamic Damping	14
3.1.3.3 Restoring Forces	16
3.1.3.4 Propulsive Forces	16
3.1.4 Equations of Motion	16
3.2 Simulation and Control	18
3.2.1 Motion Simulation	18
3.2.1.1 Glider Mode	18
3.2.1.2 Thrust Mode	18
3.2.2 Closed Loop Control	20
4 PATH PLANNING	27
4.1 Planar Dubins Curves	28
4.2 3D Path Planning	30
4.3 Projecting from Different Vertical Planes	33
4.4 3D Path Planning by Unfolding Dubins Surfaces	35
4.5 Motion Constraints	41
4.6 High Altitude Configuration	41
4.7 Discussion of Different Path Planning Methods	43

5	CONCLUSIONS	44
6	APPENDIX	45
	REFERENCES	51

LIST OF FIGURES

2.1	Vehicle Transparent View	7
2.2	Shaft Seal Section View	9
2.3	Adapter	10
3.1	Linear motion in glide operation vs inputs: weight (red), and position of C.O.G. (blue).	19
3.2	Helical path in glide operation vs inputs: weight (red), and rudder angle δr (blue).	20
3.3	Linear dive in thrust operation vs input: stern angle δs	21
3.4	Circular motion in thrust operation vs input: rudder angle δr	22
3.5	Stabilization of heading speed	24
3.6	Steering control of the AUV in the horizontal plane	25
3.7	Dive control of the AUV in the vertical plane	26
4.1	Dubins possible configurations	28
4.2	Horizontal (blue) and vertical (red) path projections	31
4.3	Example of a 3D generated path	33
4.4	Horizontal and Vertical Paths with Plane Π	34
4.5	Example of Non-Intersecting Horizontal and Vertical Paths Extrusions	36
4.6	3D Path Example ($x = 4, y = 5, z = 3, \psi = 90 \text{ deg}, \theta = 0 \text{ deg}$)	39
4.7	3D Path Example ($x = 4, y = 5, z = 3, \psi = -45 \text{ deg}, \theta = 0 \text{ deg}$)	39
4.8	3D Path Example ($x = -4, y = 5, z = 3, \psi = 210 \text{ deg}, \theta = 0 \text{ deg}$)	40
4.9	3D Path Example ($x = 4, y = 1, z = 3, \psi = -45 \text{ deg}, \theta = 0 \text{ deg}$)	40
4.10	Example of a High Altitude path	42

LIST OF TABLES

2.1 Parameters of the Vehicle	7
---	---

CHAPTER 1

INTRODUCTION

The fascinating world beneath the sea has triggered human curiosity for seeking out methods for its exploration. From manned dives at relatively shallow depths to submarines and modern Autonomous Underwater Vehicles (AUVs) at deeper depths, man continued to find innovative ways to explore the underwaters. More recently, environmental concerns have made underwater exploration more relevant. In fact, this is a drudging and repetitive type of work, which is ideally suited for AUVs because of: (1) their ability to access critical and dangerous regions, (2) low operation cost, and (3) improved data quality.

AUVs are unmanned robotic platforms, which perform underwater missions controlled by onboard computers with no need for interaction with a human operator [2]. They have proved to be a reliable platforms for acquiring oceanic data and sending this data via satellite, eliminating the need of any physical connection. In fact, their utility has lead to their usage in several scientific and commercial applications. Our development of an AUV is driven by a maritime application to perform geo-tagged sampling for pollution and environmental assessment. Historically, the design of an AUV followed one of two paradigms, (1) either to have it short, quickly maneuverable and driven by a propeller —which we will refer to as thrusters— or (2) to have a long configuration, which is not as easily maneuverable, but requires no propeller and glides up and down the ocean depths by varying its buoyancy.

Throughout the past few decades, various thruster and glider designs have been proposed and implemented. The Odyssey II [3], was developed to perform

under-ice mapping and deep-survey missions. The REMUS [24][22] was developed to collect environmental data and study marine ecosystems. The IsIMI [18] is another example of a small thruster designed to be handled by one or two operators. Generally, thrusters are reliable when efficiency of motion and good maneuverability are to be considered, but are limited to performing only short-range and low-endurance missions due to their onboard limited power supply. On the other hand, gliders can navigate for months and cover ranges up to thousands of miles on a single charge. Minimizing the power consumption of gliders comes at the expense of poor steerability due the gliders' long profile [2]. Various approaches for modeling the dynamics of AUVs are described in literature for thrusters [12] [13] [11] [22] and [9], and for gliders [17] and [14]. In these works, the dynamic modeling deals with propelled AUVs and gliders separately.

In light of this information, it would seem only natural that a hybrid AUV would take advantages of the features of both designs and reduce the shortcomings of each. Integrating such features into one system would hypothetically result in an underwater platform with a long range and endurance, but capable in the same time of performing complex maneuvers when needed. In a long range mission, a hybrid AUV would only rely on its buoyancy to cover such large distances. Using the thruster in such mission would be a sacrifice of onboard carried power supply. On the other hand when high speed and sharp turns are required, the thruster and steering wings would come in handy.

The PETREL [25] is a winged hybrid AUV, similar to the one proposed in this paper. In propulsion mode, the PETREL utilizes a single thruster and four actuated hydrodynamic fins, whereas in the gliding mode, it uses a ballast pump and two fixed wings. In Wang et al.[25] only the dynamic model and motion simula-

tions of the vehicle are presented without getting into a control method. The Folaga which is presented by Caiti and Calabro [5] is an example of a torpedo-shaped hybrid AUV with no hydrodynamic wings or fins. The design of the Folaga is based upon two things: (1) jet pumps to move along the surge and sway axes, and (2) buoyancy-change as well as internal mass movement for pitch and depth control. A main shortcoming of the above mentioned hybrids is the mismatch between the dynamic simplified model and the complete vehicle dynamics. Caiti and Calabro [5] addressed this issue by proposing a backstepping controller with fuzzy adaptation to cope with this problem.

As for motion planning, we take recourse to Dubins approach of generating minimal time planar trajectories which is implemented on wheeled mobile robots ([8] [1]). Such type of curves have been used in the path planning of underwater gliders, as shown in Mahmoudian[19]. In an oversimplified manner, the glider's path was projected on the horizontal plane neglecting any vertical component of motion. Time-optimal trajectories for a Dubins airplane were discussed in Chitsaz and LaValle[6] by using a simplified airplane model which neglects the pitch coordinate (θ). Chitsaz and LaValle [6] and Pachikara et al. [20] considered the Dubins airplane model to be just like a Dubins car model with an added altitude coordinate (z) only.

1.1 Thesis Contribution

In our work we provide a kinematic as well as a dynamic simulation model describing all forces acting on the vehicle. We show some open loop motion scenarios in addition to a closed loop sliding mode techniques to control the heading and steering velocities. We address the shortcomings of Mahmoudian[19], and Chitsaz and LaValle[6] by proposing several three dimensional Dubins type path planning

methods which take into account both altitude coordinate (z) and the pitch rotation (θ).

1.2 Thesis Outline

This thesis proceeds as follows: Chapter 2 introduces conceptual design of the hybrid AUV, with a brief overview of the mechanical design. Chapter 3 provides the kinematic and dynamic models with the governing equations of motion, in addition to open and closed loop simulations of some of the vehicle's maneuvers. Chapter 4 restates the Dubins 2D curves and introduce a method of solving the inverse problem in 2D. Chapter 5 presents three novel methods for finding efficient motion trajectories in 3D. Chapter 6 concludes the thesis with a discussion and suggestions for future development.

CHAPTER 2

MECHANICAL DESIGN

In this chapter we provide the design of a hybrid AUV, discussing briefly the features of the vehicle and the concept of the design.

2.1 Design Concept

The hybrid AUV presented here is based on integrating features of thrusters and gliders into a system capable of gliding due to its buoyancy changes, and/or thrusting via a propeller. The proposed design is shown in Fig. 2.1 and is a torpedo-like vehicle with a propeller in the aft section, and steerable control surfaces to control the pitch and yaw rotations. A buoyancy engine provides the ability to control the buoyancy of the body by shifting an amount of water in and out a ballast tank located inside the body, and thus controlling the vertical motion. Adding two large span wings creates horizontal forces that move the vehicle forwards during a dive or an ascent. The advantage of having a hybrid AUV is minimized power consumption and extended operation periods while maintaining good maneuverability due to thrust and control wings.

The shape of the hull is constrained by the hydrodynamic characteristics of the AUV, where a torpedo-like shape insures low drag coefficient ratios [2]. The vehicle hull is composed of four sections (see in Fig. 2.1):

- The Nose or the front hull is an aluminum cylinder closed with a hemi-

spherical-like top. The nose is designed to house a sonar transponders, and other scientific payload sensors, which are selected according to the nature of the mission. The AUV may have many applications thus the scientific payload of the vehicle is modular and can be changed due to the mission the AUV is assigned to do. There are however many acoustic and non-acoustic payloads which can span a range of applications for measuring water qualities.

- The middle hull section the buoyancy engine of the vehicle. The buoyancy engine also called buoyancy pump or ballast pump, is a device used to control the buoyancy of the vehicle. The piston ballast is one of the most common and easy diving methods applied in submarine design. A piston ballast tank consists of a cylinder and a movable piston, which works as a syringe pump displacing water inside and out of the vehicle's body. The piston of the cylinder is moved by a linear actuator which could be electrically controlled.
- The rear chamber of the vehicle or the rear hull is designed to house batteries, CPU, electronics, GPS antenna, and servo actuators to control the rudder planes.
- The tail cone houses the thruster, which which is a DC motor that drives a propeller fan.

The modular design of the vehicle makes it possible to add any other extra payload section. The vehicle parameters are shown in Table 2.1. The dimensions and weight of the vehicle allows it to be easily deployed and retrieved from a small boat. The hull is a pressure housing made from aluminum 6061-T6 alloy, which is characterized by good corrosion resistance properties, and a yield strength of $S_y = 275 \text{ MPa}$, which would allow the vehicle to resist a hydrostatic pressure of 40 bars (400 m depth).

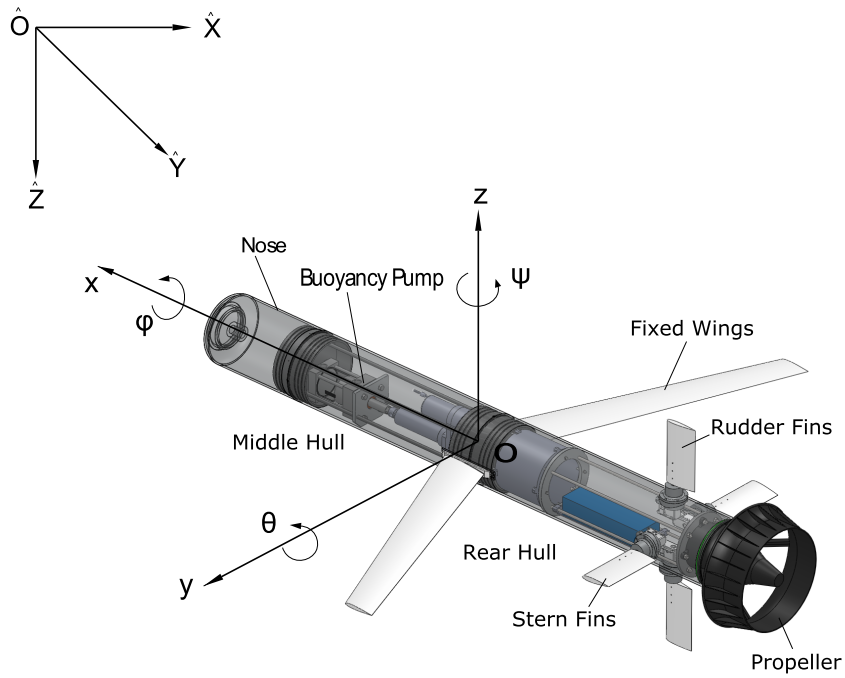


Figure 2.1: Vehicle Transparent View

Table 2.1: Parameters of the Vehicle

Length	200.9 cm
Diameter	21.4 cm
Weight	72.5 Kg
Max. Speed	2 m/s
Hull	Aluminum 6061-T6
Max. Operating Depth	200 m
Motor	Hollis High Torque Brushed Motor
Propulsion	27.6V - 16 Ah - NiMh
Communication	Iridium 9602

2.2 Design Features

2.2.1 Wings

Four control wings are installed in the rear hull section, driven by servo actuators. Two rudders or vertical wings provide the yaw rotation about the z axis of the body, which allows the vehicle moving left or right. Another two horizontal wings which control the pitch rotation of the vehicle about the y axis. The profile

shapes of these wings follow the standard NACA 0012 section with an aspect ratio of 4. The NACA 0012 is a symmetric profile insuring very low drag and no lift at zero angle, in addition being easily machined. Another two fixed wings are attached to the body providing extra lift force during the vehicle's gliding operations.

2.2.2 Pressure Shaft Sealing

A shaft sealing connects the control planes to the internal actuator motor which is designed to prevent sea water to leak inside the hull, and enable the rotation of the shaft by the actuator under external pressure. The shaft seal is made up of internal parts consisting of a single shaft, two ball bearings, two dynamic seals with one backup ring, a face seal, four pins, a plastic spacer, and a circlip shown in Fig. 2.2. The fixture ring is a piece of aluminum welded to the rear hull. A top external section or a cap is screwed on the fixture ring. Two dynamic seals, one with a backup ring are mounted in the cap to ensure the seal between the cap and shaft. A ball bearing is also mounted inside the cap to allow the shaft to rotate freely. A second bearing is installed on the shaft, where a plastic spacer is used to maintain the bearings stationary. The lower internal section is the motor bracket, which is a piece of aluminum holding the motor actuator, and fixed to the fixture ring.

2.2.3 Adapters and Sealing

The joints between the chambers are adapters or circumferential joints fitted down inside the end of the cylinder can, like a piston in a cylinder. O-rings are sandwiched between the adapter and the inside of the cylinder to create a waterproof seal. The seal is achieved when external water pressure compresses the diameter of the can slightly, squeezing the O-rings. The surfaces of the cylinder and the adapters are machined with a smooth surface quality and free of sharp edges and thus ensuring

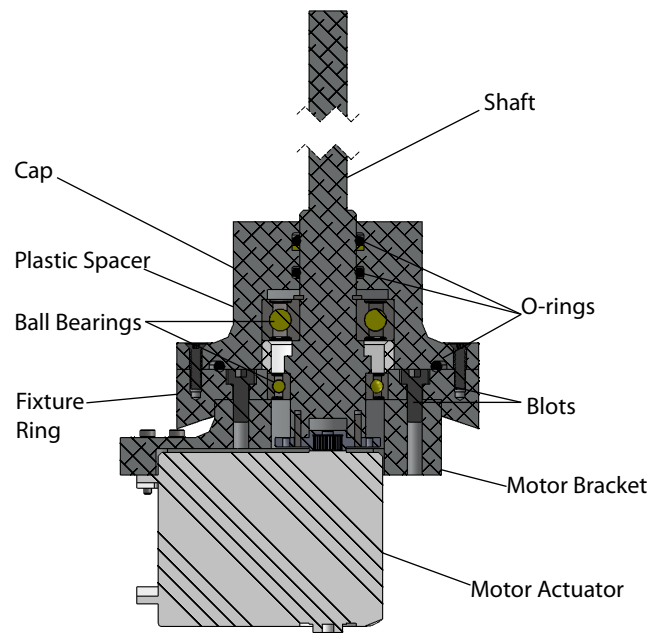


Figure 2.2: Shaft Seal Section View

a transitional fit structure and a good leak-proof seal.

2.2.4 Other Components

- The power supply of the vehicle is a 27.6V - 16 Ah - NiMh - 23 cells battery pack.
- Four servo actuators are used to control the rudder and stern wings of the vehicle. These actuators acquire a very fine resolution and a high stall torque.
- A short burst data transceiver is used for communication. This device is used to communicate with the vehicle directly through satellite, while the vehicle is on the surface.
- A sonar transponder and an inertial measurement unit (IMU) are used for localizing the vehicle.

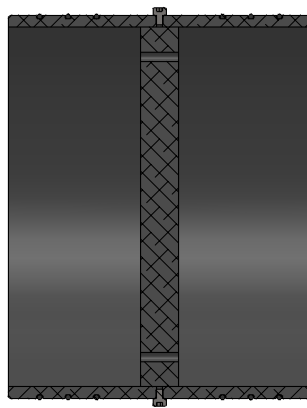
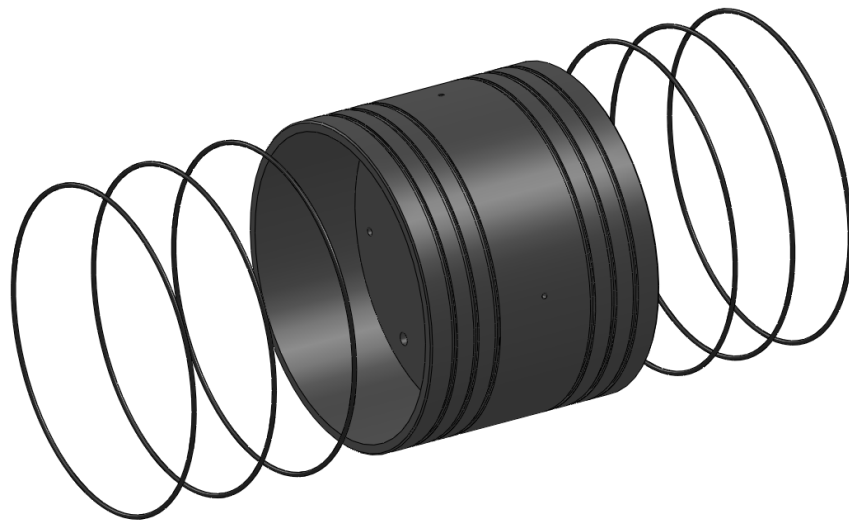


Figure 2.3: Adapter

CHAPTER 3

MODELING SIMULATION AND CONTROL

3.1 System Modeling

In this section the coordinate frames are defined and the transformations between these frames are computed. The kinematics of the system is studied, along with the rigid body dynamics and hydrodynamic forces applied on the vehicle. Finally, the governing equations of motion are derived.

3.1.1 *Coordinate Frames and Transformations*

Two coordinate frames are used to describe the kinematic model of an underwater vehicle, the Earth frame or inertial frame and the body-fixed frame (Fig. 2.1). The inertial frame $(\hat{O}, \hat{X}, \hat{Y}, \hat{Z})$ is fixed to a point at the ocean surface with vector (\hat{O}, \hat{Z}) orthogonal and pointing down to the water surface. This frame is used to express the posture of the vehicle's center of mass $\eta = [\eta_1^T, \eta_2^T]^T$, where $\eta_1 = [x, y, z]^T$ and $\eta_2 = [\phi, \theta, \psi]^T$ are the position and orientation vectors respectively. The body-fixed frame (o, x, y, z) is connected to the vehicle's center of buoyancy (or geometric center), with vector (o, x) pointing out through the nose of the vehicle. The body frame is used to express the vehicle's velocities $\nu = [\nu_1^T, \nu_2^T]^T$, where $\nu_1 = [u, v, w]^T$ and $\nu_2 = [p, q, r]^T$ represent the linear and angular velocity vectors respectively. We also define the position of the mass center with respect to the geometric center to be $[x_G, y_G, z_G]^T$. The transformation from the body-fixed frame to the inertial frame as stated by Fossen [12]:

$$\dot{\eta} = \begin{bmatrix} J_1 & 0 \\ 0 & J_2 \end{bmatrix} \nu \quad (1)$$

where:

$$J_2 = \begin{bmatrix} 1 & s_\phi t_\theta & c_\phi t_\theta \\ 0 & c_\phi & -s_\phi \\ 0 & s_\phi/c_\theta & c_\phi/c_\theta \end{bmatrix} \quad (2)$$

$$J_1 = \begin{bmatrix} c_\psi c_\theta & -s_\psi c_\phi + c_\psi s_\theta s_\phi & s_\psi s_\phi + c_\psi c_\theta s_\phi \\ s_\psi c_\theta & c_\psi c_\phi + s_\psi s_\theta s_\phi & -c_\psi s_\phi + s_\psi s_\theta c_\phi \\ -s_\theta & c_\theta s_\phi & c_\theta c_\phi \end{bmatrix} \quad (2)$$

3.1.2 Rigid Body Dynamics

The six degrees of freedom rigid-body equations of motion are derived by applying the *Newtonian* and *Lagrangian* formalism, given in Fossen [12], and are repeated here for convenience:

$$\begin{aligned} m[\dot{u} - vr + wq - x_G(q^2 + r^2) + y_G(pq - \dot{r}) + z_G(pr + \dot{q})] &= X \\ m[\dot{v} - wp + ur - y_G(r^2 + p^2) + z_G(qr - \dot{p}) + x_G(qp + \dot{r})] &= Y \\ m[\dot{w} - uq + vp - z_G(p^2 + q^2) + x_G(rp - \dot{q}) + y_G(rq + \dot{p})] &= Z \\ I_x \dot{p} + (I_z - I_y)qr - (\dot{r} + pq)I_{xz} + (r^2 - q^2)I_{yz} + (pr - \dot{q})I_{xy} \\ &\quad + m[y_G(\dot{w} - uq + vp) - z_G(\dot{v} - wp + ur)] = K \quad (3) \\ I_y \dot{q} + (I_x - I_z)rp - (\dot{p} + qr)I_{xy} + (p^2 - r^2)I_{zx} + (qp - \dot{r})I_{yz} \\ &\quad + m[z_G(\dot{u} - vr + wq) - x_G(\dot{w} - uq + vp)] = M \\ I_z \dot{r} + (I_y - I_x)pq - (\dot{q} + rp)I_{yz} + (q^2 - p^2)I_{xy} + (rq - \dot{p})I_{zx} \\ &\quad + m[x_G(\dot{v} - wp + ur) - y_G(\dot{u} - vr + wq)] = N \end{aligned}$$

These equations can be written as a simplified matrix form:

$$M_{RB}\dot{\nu} + C_{RB}(\nu)\nu = \tau_{RB}, \quad (3)$$

where M_{RB} is the rigid-body inertia matrix, C_{RB} is the Coriolis and centripetal matrix, and τ_{RB} is the total forces and moments acting on the body.

3.1.3 Hydrodynamic Forces and Moments

As stated by Faltinsen [10] the hydrodynamic forces and moments acting on a rigid body are expressed as radiation-induced forces, and propulsion forces. The radiation induced forces and moments are identified in three sub-categories: (1) *Added mass* due to the inertia of surrounding fluid, (2) *Radiation induced potential damping*, and (3) *Restoration forces* due to Archimedes.

3.1.3.1 Added Mass

Added mass is induced due to the oscillation of fluid with different particle fluid particle amplitude in phase with the forces harmonic motion of the vehicle, as defined in [12]. Added mass coefficients are derived using Kirchoff's energy equations, and expressed in terms of added mass inertia matrix M_A , and added mass coriolis and centripetal matrix C_A . Thus the forces and moments acting on the vehicle are given as $M_A\dot{\nu} + C_A\nu$, which is expanded in the following form:

$$\begin{aligned}
X_A &= X_{\dot{u}}\dot{u} + Z_{\dot{w}}w\dot{q} + M_{\dot{w}}\dot{q}^2 - Y_{\dot{v}}vr - N_{\dot{v}}r^2; \\
Y_A &= Y_{\dot{v}}\dot{v} + N_{\dot{v}}\dot{r} + X_{\dot{u}}ur - Z_{\dot{w}}wp + M_{\dot{w}}qp; \\
Z_A &= Z_{\dot{w}}\dot{w} + M_{\dot{w}}\dot{q} + X_{\dot{u}}uq + Y_{\dot{v}}vp + N_{\dot{v}}rp; \\
K_A &= K_{\dot{p}}\dot{p} + Z_{\dot{w}}wv + M_{\dot{w}}qv - Y_{\dot{v}}vw - N_{\dot{v}}rv + N_{\dot{v}}vq + N_{\dot{r}}rq - M_{\dot{w}}wr - M_{\dot{q}}qr; \\
M_A &= M_{\dot{w}}\dot{w} + M_{\dot{q}}\dot{q} - (Z_{\dot{w}} - X_{\dot{u}})wu - M_{\dot{w}}qu - N_{\dot{v}}vp + (K_{\dot{p}} - N_{\dot{r}})rp; \\
N_A &= N_{\dot{v}}\dot{v} + N_{\dot{r}}\dot{r} - (X_{\dot{w}} - Y_{\dot{u}})uv + M_{\dot{w}}wp - (K_{\dot{p}} - M_{\dot{q}})pq + N_{\dot{v}}ur.
\end{aligned}$$

For axial and rolling added mass coefficients, and empirical formula provided in Blevins[4]:

$$X_{\dot{u}} = -\frac{4\alpha\rho\pi}{3} \left(\frac{l}{2}\right) \left(\frac{d}{2}\right)^2; \quad K_{\dot{p}} = \int_{x_{fin1}}^{x_{fin2}} \frac{2}{\pi} \rho a^4 dx; \quad (5)$$

where ρ is the water density, l the axial length of the vehicle, d the vehicle's diameter, α is a geometrical parameter dependent on the vehicle's l/d ratio, and a is the fin height above the vehicle centerline.

The crossflow added masses can be obtained by applying strip theory for a slender body vehicle found in [18] (See Appendix).

3.1.3.2 Hydrodynamic Damping

- Body Drag, similar to added mass, drag is also divided into axial, crossflow, and rolling drag forces. Axial drag is calculated by Hoerner [15] based on the following empirical formula:

$$X = -\left(\frac{1}{2}\rho c_d A_f\right)u|u| = X_{u|u}|u| \quad (4)$$

where c_d is the drag coefficient, ρ (kg/m^3) is the water density, and A_f (m^2) is the frontal area of the body.

Crossflow and rolling drag are also derived empirically from Hoerner[15] using a method similar to strip theory method used to calculate the added mass. The total drag could be approximated as the sum of drag forces and moments on the two-dimensional cylindrical vehicle. Crossflow drag coefficients are stated in the Appendix.

- Body Lift is a result of a body moving through a fluid at an angle of attack, causing a difference in pressure between the upper and lower sections of the body. This pressure drop is modeled as a force concentrated at the center of pressure of the vehicle. Hoerner and Borst [16] provides a reliable empirical formula to compute the lift forces and moments:

$$L_{body} = -\frac{1}{2}\rho A_p c_{yd\beta} uv, \quad M_{body} = L_{body} x_{cp}, \quad (5)$$

where x_{cp} (m) is the position of center of pressure. A_p (m^2) is the hull projected area of the vehicle hull and $c_{yd\beta}$ the body lift slope.

- The attitude and sideways maneuvering of the vehicle is controlled by two horizontal fins, or stern wings, and two vertical fins, or rudders, respectively. For the vehicle control fins, as for the body lift, are defined by Whicker and Fehlner [26] as:

$$L_{fin} = -\frac{1}{2}\rho A_p c_L S_{fin} \delta_e v_e^2, \quad M_{fin} = L_{fin} x_{fin} \quad (6)$$

where c_L is the fin lift coefficient, S_{fin} (m^2) the fin planform area, δ_e (rd) the effective fin angle in radians, v_e (m/s) the effective fin velocity, and x_{fin} (m) the axial position of the fin position in body-fixed reference coordinates.

3.1.3.3 Restoring Forces

The hydrostatic restoring forces are simply the gravitational and buoyant forces. The weight of a submerged body is defined as $W = mg$, while the buoyant force according to Archimedes principle is defined as $B = \rho g \nabla$, where g (m/s^2) is the gravitational acceleration, ∇ (m^3) is the volume of the vehicle [12].

3.1.3.4 Propulsive Forces

The propeller is considered as a source of constant thrust and torque. The thrust is assumed to match the axial drag and the propeller torque to match the hydrostatic roll moment.

3.1.4 Equations of Motion

Combining the vehicle's rigid-body dynamics with the equations of hydrodynamic forces and moments acting on the vehicle results in complete six degrees of freedom combined nonlinear equations of motion:

$$M\dot{\nu} + C(\nu)\nu + D(\nu)\nu + g(\eta) = \tau \quad (7)$$

Rearranging this equation to get:

$$M\dot{\nu} = \sum F_{ext} \quad (8)$$

Following the SNAME convention [22], the sum of external forces can be expressed as:

Surge:

$$\begin{aligned}
X = & -(W - B)\sin\theta + X_{uu}u|u| + (X_{wq} - m)wq \\
& + (X_{qq} + mx_G)q^2 + (X_{vr} + m)vr + (X_{rr} + mx_G)r^2 \\
& - my_Gpq - mz_gp r + X_{prop};
\end{aligned} \tag{9}$$

Sway:

$$\begin{aligned}
Y = & (W - B)\cos\theta\sin\phi + Y_{vv}v|v| + Y_{rr}r|r| + Y_{uv}uv \\
& + (Y_{wp} + m)wp + (Y_{ur} - m)ur - (mz_G)qr \\
& + (Y_{pq} - mx_G)pq + Y_{uu\delta}r u^{2*}\delta r;
\end{aligned} \tag{10}$$

Heave:

$$\begin{aligned}
Z = & (W - B)\cos\theta\cos\phi + Z_{ww}w|w| + Z_{qq}q|q| + Z_{uw}uw \\
& + (Z_{uq} + m)uq + (Z_{vp} - m)vp + mz_G(p^2 + q^2) \\
& + (Z_{rp} - mx_G)rp + Z_{uu\delta}s u^2\delta s;
\end{aligned} \tag{11}$$

Roll:

$$\begin{aligned}
K = & -W(y_G\cos\theta\cos\phi + z_G\cos\theta\sin\phi) + K_{pp}p|p| \\
& - (I_{zz} - I + yy)qr - mz_G(wp + ur) + K_{prop};
\end{aligned} \tag{12}$$

Pitch:

$$\begin{aligned}
M = & -W(z_G\sin\theta + x_G\cos\theta\cos\phi) + M_{ww}w|w| + M_{qq}q|q| \\
& + (M_{rp} - (I_{xx} - I_{zz}))rp + mz_G(vr - wq) \\
& + (M_{uq} - mx_G)uq + M_{uw}uw \\
& + (M_{vp} + mx_G)vp + M_{uu}\delta s u^2\delta s;
\end{aligned} \tag{13}$$

and

Yaw:

$$\begin{aligned}
N = & -W(x_G\cos\theta\sin\phi + y_G\sin\theta) + N_{vv}v|v| \\
& + N_{rr}r|r| + N_{uv}uv + (N_{pq} - (I_{yy} - I_{xx}))pq \\
& + (N_{wp} + mx_G)wp + (N_{ur} - mx_G)ur + N_{uu\delta}r u^2\delta r.
\end{aligned} \tag{14}$$

3.2 Simulation and Control

In this section, the equations of motion derived above are solved numerically for various inputs. The results are plotted and discussed, and will be used later for the path planning problem in Section 5.

3.2.1 *Motion Simulation*

The hybrid AUV is usually operated in two modes, the glide and the thrust modes.

3.2.1.1 Glider Mode

For gliding operations the vehicle uses its buoyancy engine to vary the buoyancy of the body, and shifts its center of gravity along its surge axis. A positive buoyancy and negative position of the center of mass x_G , result in a forward ascend of the vehicle, while a negative buoyancy and a positive x_G , creates a forward dive. Switching between these two configurations while maintaining zero deflection of the vertical and horizontal rudders leads the vehicle to glide linearly in a zig-zag like motion as shown in Fig. 3.1. In gliding mode the vehicle's heading velocity is relatively low ($0.5m/s$).

Using its vertical rudders to create a moment about the yaw axis while gliding, which result in a helical pattern of motion shown in Fig. 3.2.

3.2.1.2 Thrust Mode

In thrust mode the vehicle relies on a single thruster, and steered by two vertical and two horizontal fins or rudders. Provided these inputs, the vehicle is ma-

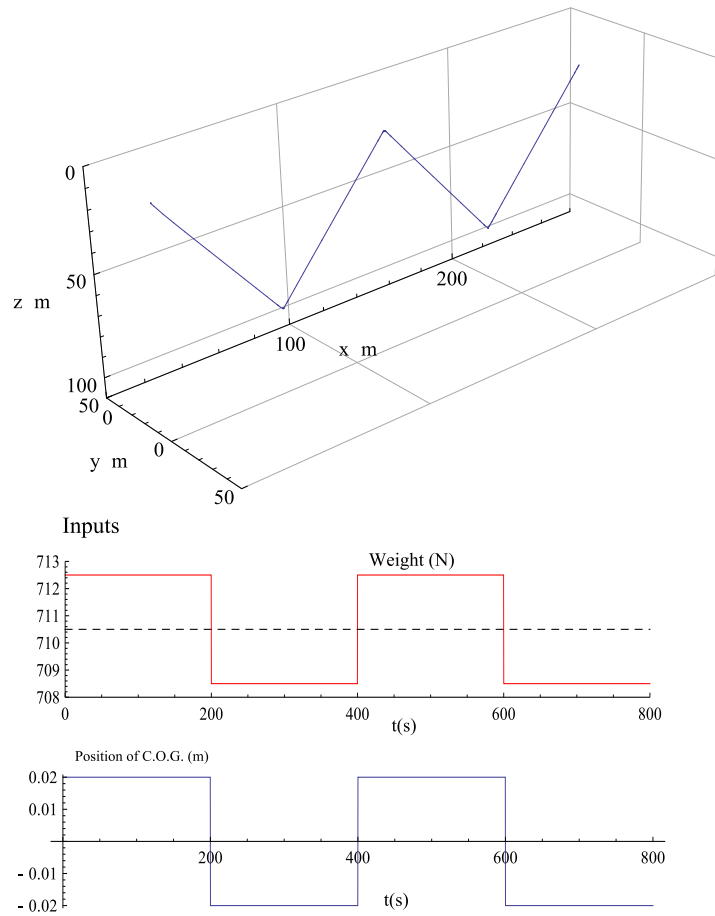


Figure 3.1: Linear motion in glide operation vs inputs: weight (red), and position of C.O.G. (blue).

neuverable in four configurations: (1) Linear horizontal motion, by simply applying only thrust without any rudder angle deflections; (2) linear dive, which is achieved by using the horizontal rudders to let the vehicle dive vertically up or down the water column by the action of the pitching moment produced about the vehicle's y -axis. Fig. 3.3 shows the vehicle's motion in the xz plane;

(3) circular motion in a plane, is obtained by deflecting the vertical rudders produces a yawing moment about the vehicle's z -axis. Fig. 3.4 shows the vehicle's motion in the xy plane;

(4) helical motion, which is obtained by applying an angle to both vertical and horizontal rudder planes.

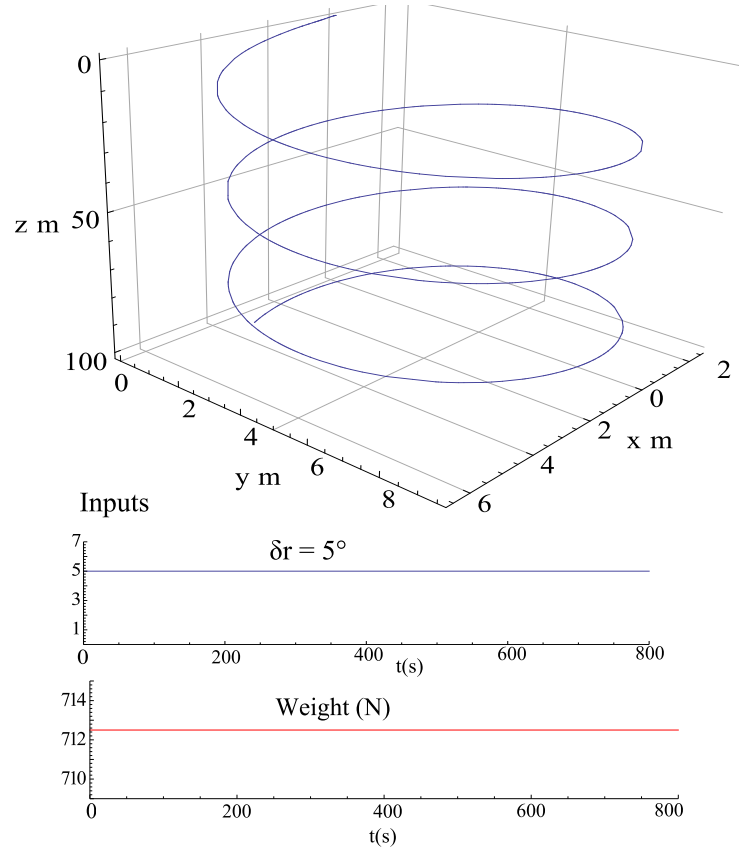


Figure 3.2: Helical path in glide operation vs inputs: weight (red), and rudder angle δr (blue).

3.2.2 Closed Loop Control

In this section we apply the method of sliding mode control [12] [4], to drive the vehicle along elementary sub-trajectories. These sub-trajectories are simply arcs of circles with minimum allowable radii, and straight lines, these sub-trajectories are essential for our proposed path planning algorithm. To achieve that, we need to separate the system into three independent or slightly interacting subsystems functions of the heading speed, steering and diving controls respectively. Each subsystem is referred to as Single Input Multi State system (SIMS), with only a single active input [4].

We consider a kinematic system that is written as the form

$$\dot{x} = Ax + bu + f(x) \quad (15)$$

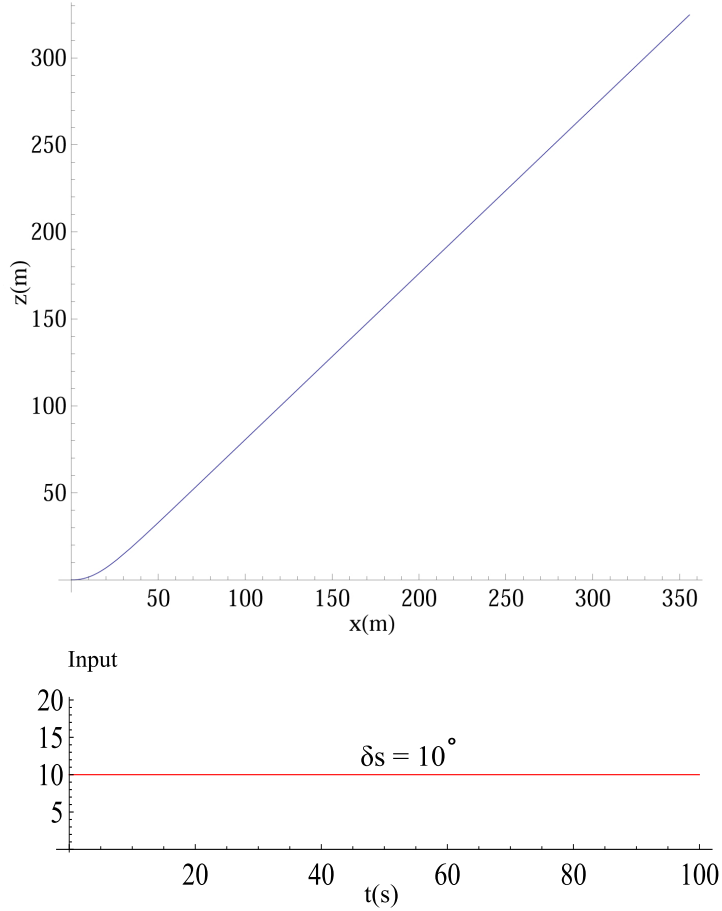


Figure 3.3: Linear dive in thrust operation vs input: stern angle δ_s

where x is the state, u the input, and $f(x)$ is a function representing the nonlinearities such as disturbances and unmodelled dynamics. [4] defined the sliding surface to be

$$\sigma(\tilde{x}) = h^T \tilde{x} \quad (16)$$

where $\tilde{x} = x - x_d$ is the tracking error, and h is a constant vector interpreted later. Let $A_c = A - bk^T$, k is a feedback gain vector which can be determined by pole-placement technique. This is done by specifying the closed loop poles of matrix A_c , and thus solving for the values of vector k [12]. Then h could be determined as the right eigenvector of A_c for $\lambda = 0$. The control input is then chosen to be of the form

$$u = -k^T x + (h^T b)^{-1} [h^T \dot{x} - h^T f(x) - \eta \tanh(u/\phi)] \quad (17)$$

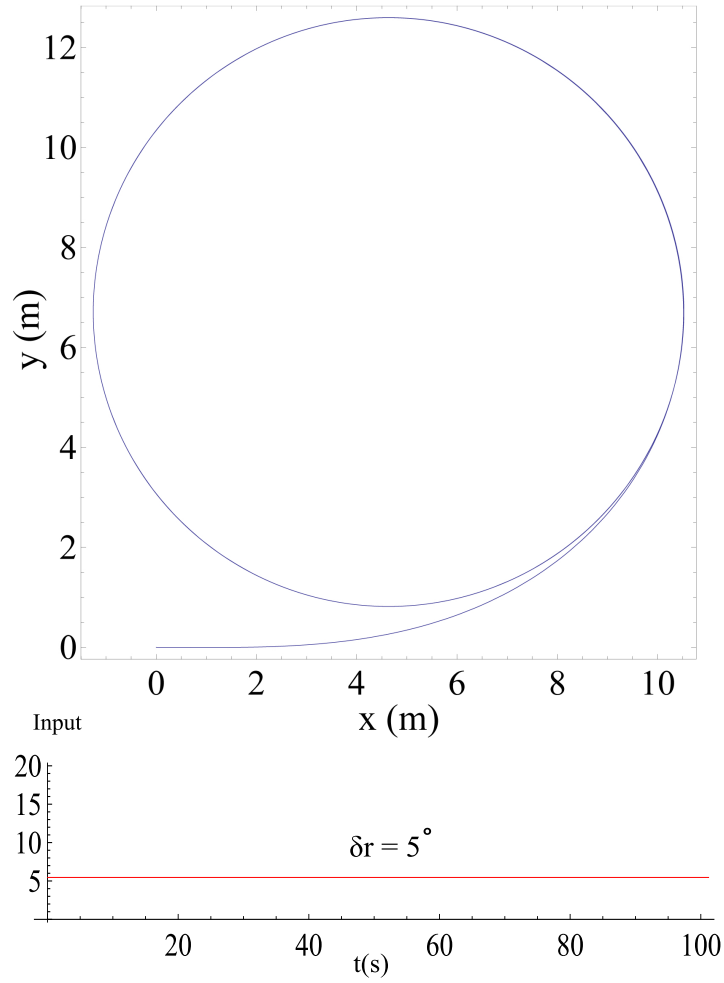


Figure 3.4: Circular motion in thrust operation vs input: rudder angle δr

where η is a constant chosen large enough to overcome the destabilizing effects of the unmodelled dynamics, and ϕ is parameter used to prevent chattering and maintain the continuity of motion along the sliding surface [4].

Hence the equations of the three subsystems and their corresponding inputs can be written as the following:

1. Heading Speed Control: the speed equation can be written in this form

$$(m - X_{\dot{u}})\dot{u} + X_{|u|u}|u|u = X_{|n|n}|n|n + f(u, n) \quad (18)$$

where $X_{|n|n}$ is the propeller force coefficient and $f(u, n)$ represents the un-

modelled dynamics. The sliding surface is selected as:

$$\sigma = \bar{u} = u - u_d \quad (19)$$

and the control input is selected as:

$$|n|n = \frac{1}{X_{|n|n}} [X_{|u|u} u |u| + (m - X_{\dot{u}}) \dot{u}_d - (m - X_{\dot{u}}) \eta \tanh(\sigma/\phi)]$$

2. Steering Control: The steering linear equations of motion are given as:

$$\begin{bmatrix} \dot{v} \\ \dot{r} \\ \dot{\psi} \end{bmatrix} = \begin{bmatrix} a_{11} & a_{12} & 0 \\ a_{21} & a_{22} & 0 \\ 0 & 1 & 0 \end{bmatrix} \begin{bmatrix} v \\ r \\ \psi \end{bmatrix} + \begin{bmatrix} b_1 \\ b_2 \\ 0 \end{bmatrix} \delta_r \quad (20)$$

The sliding surface is selected as:

$$\sigma_r = h_1 v + h_2 (r - r_d) + h_3 (\psi - \psi_d) \quad (21)$$

and the steering control law is:

$$\delta_r = -k_1 v - k_2 r + \frac{1}{\beta_0} [h_2 \dot{r}_d + h_3 \dot{\psi}_d - \eta \tanh(\sigma_r/\phi)] \quad (22)$$

where $\beta_0 = h^T b$.

3. Pitch-Depth Control: The reduced linear model is expressed as:

$$\begin{bmatrix} \dot{q} \\ \dot{\theta} \\ \dot{z} \end{bmatrix} = \begin{bmatrix} \frac{M_q}{I_y - M_{\dot{q}}} & -\frac{(z_G - z_B)W}{I_y - M_{\dot{q}}} & 0 \\ 1 & 0 & 0 \\ 0 & -u_0 & 0 \end{bmatrix} \begin{bmatrix} q \\ \theta \\ z \end{bmatrix} + \begin{bmatrix} \frac{M_{\delta}}{I_y - M_{\dot{q}}} \\ 0 \\ 0 \end{bmatrix} \delta_s \quad (23)$$

The sliding surface is selected as:

$$\sigma_s = h_1(q - q_d) + h_2(\theta - \theta_d) + h_3(z - z_d) \quad (24)$$

and the pitch control law is:

$$\delta_s = -k_1q - k_2\theta + \frac{1}{\beta_0}[h_1q_d + h_2\theta_d - \eta \tanh(\sigma_s/\phi)] \quad (25)$$

As mentioned earlier, the sliding mode method described above is used to track the vehicle along a Dubins path composed of a concatenation of circles and straight lines (discussed in the next section). To track the vehicle along a straight line, we simply need to stabilize the heading velocity to a constant value, and any angular velocity (steering or diving) should be maintained to zero. While for achieving a circular path with a minimal radius in the horizontal plane, both the heading velocity (u) and the steering angular velocity (r) must be stabilized simultaneously to their maximum possible value. Similarly, for the diving plane, the heading velocity (u) and the pitch angular velocity (q) must be stabilized.

Fig. 3.5 shows an example of stabilizing the heading speed, where the red curve is the controlled velocity, and the dotted one is the desired value.

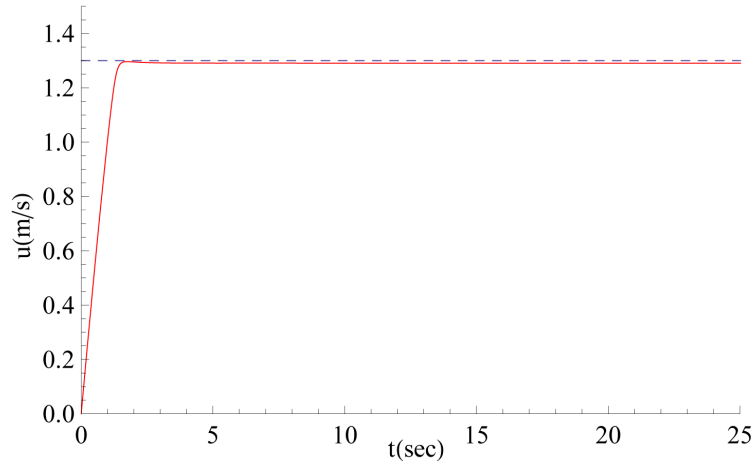


Figure 3.5: Stabilization of heading speed

A typical example of a Dubins curve in the horizontal plane, would be a concatenation of an arc of a circle, followed by a straight line, followed by another arc. Fig. 3.6 shows the controlled steering angular velocity r along three time intervals, and the trace of the path travelled by the vehicle in the horizontal plane.

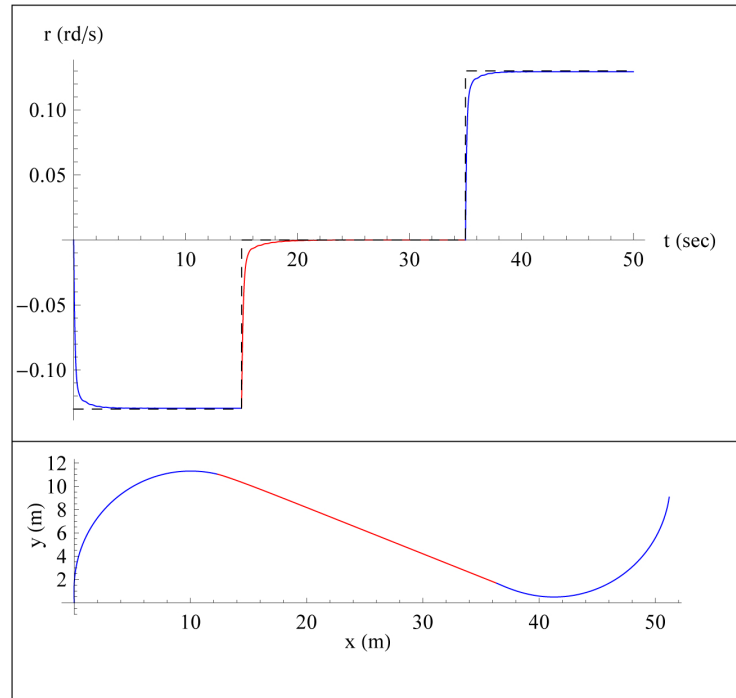


Figure 3.6: Steering control of the AUV in the horizontal plane

Fig. 3.7 shows the controlled pitch angular velocity q along three time interval, and the trace of the path travelled by the vehicle in the vertical plane.

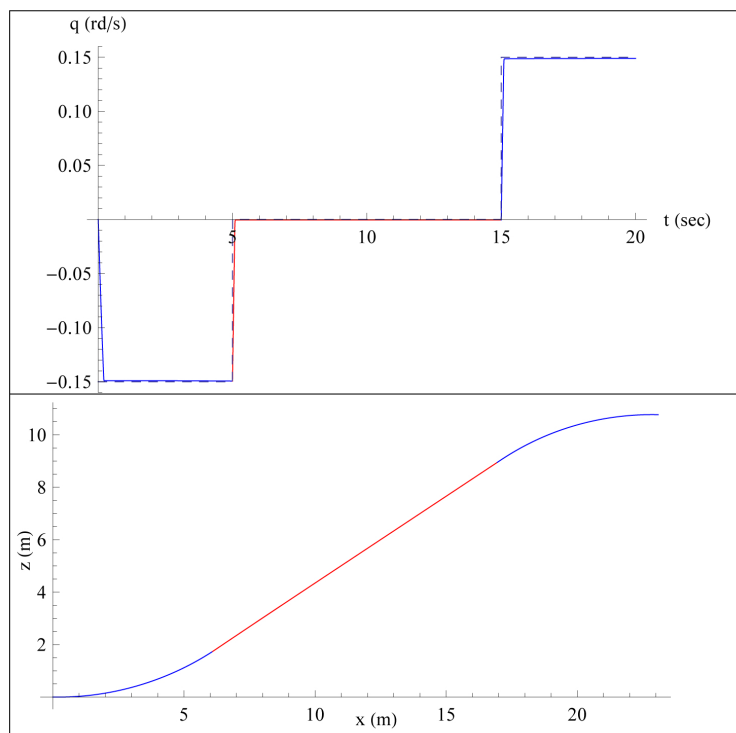


Figure 3.7: Dive control of the AUV in the vertical plane

CHAPTER 4

PATH PLANNING

Path planning techniques are used in autonomous systems for driving vehicles along trajectories which connects an initial position and orientation to a final position and orientation. Depending on the nature of the autonomous vehicle and the type of environment it lives in, the vehicle's maneuverability is determined, and so its feasible set of trajectories. The most challenging task lies in finding the set of optimal or minimal distance trajectories amongst the set of feasible ones. Autonomous underwater vehicles are capable of maneuvering in both 2-dimensional (2D) and 3-dimensional (3D) space. Without engaging any pitch/dive steering the vehicle is capable of maneuvering in a horizontal plane, similarly a vertical planar motion is acquired when no yaw steering is applied. In such cases 2D techniques could be implemented to drive the vehicle from an initial to a final configuration. On the other hand, when both pitch and yaw steering are applied together the vehicle is capable of performing 3D maneuvers.

Motion Planning Problem: *Given two vectors V_o and V_f , positioned on two different points O and P_f respectively in an n -dimensional space such that $n \in \{2, 3\}$, find a minimal length curve with a maximum curvature constraint linking points O and P_f and tangent to vectors V_o and V_f .*

In the following section, the concept of minimal length curves in a plane with a constraint on maximum curvature as proposed by mathematician L.E. Dubins in 1957 [8] is restated and derived in the form of mathematical parametric equations. Next, a method for finding efficient 3D trajectories is devised by using the 2D Dubins paths as its basis.

4.1 Planar Dubins Curves

In [8] Dubins proved that the shortest fixed speed curve in a plane with a minimum radius of curvature (R), is necessarily a continuously differentiable curve which is either a concatenation of an arc of a circle of radius R , followed by a line segment, followed by another arc of a circle of radius R (CSC); or a sequence of three arcs of circles of radius R (CCC); or a subpath of any of the two above.

Without loss of generality, we will consider the minimum radius of curvature for our robot to be a unit radius ($R = 1$); the heading angle is always measured from the (o, x) -axis of a reference frame (o, x, y) ; and the initial position to be the origin o with a zero heading angle. For any final position P_f in plane (x, o, y) , given its final heading angle ψ_f , we are able to construct four possible configurations of the Dubins path of type CSC stated as: RSL, LSR, RSR, and LSL. Where R and L represents a right and left turn respectively, and S represents a straight line. Fig. 4.1 shows all four possible configurations. Thus the optimal path is simply the one of the shortest length among of the four possible paths. To plot these curves, we

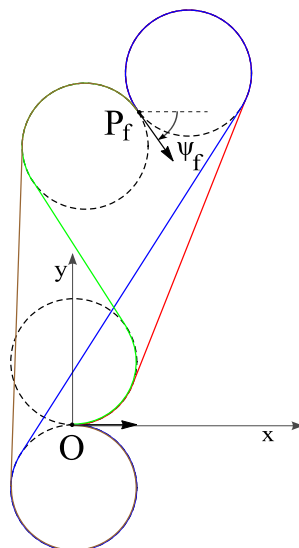


Figure 4.1: Dubins possible configurations

derived out the parametric equations of the considered curves against a parameter

s which represents the length of each partition of the path in meters, or the time that it takes to travel each partition moving in a constant unit speed.

Next, we find out the equations of a LSR type curve, the other cases are derived in a similar fashion. The equations of the considered path is given as:

- Left turn arc of a circle:

$$\begin{cases} x = \cos(s - \pi/2) \\ y = \sin(s - \pi/2) + 1 \end{cases} \quad (15)$$

where $s \in \{0, a\}$, and a is the length of the first arc, or the angle formed by this arc (considering $R = 1$).

- Straight line:

$$\begin{cases} x = (s - a) + \cos(a - \pi/2) \\ y = \tan[a](s - a) + \sin(a - \pi/2) + 1 \end{cases} \quad (16)$$

where $s \in \{a, a + c \cos(a)\}$, and c is the length of the straight line.

- Right turn arc of a circle

$$\begin{cases} x = \cos(-s + a + \pi/2 + (a + c \cos[a])) + c \cos(a) \\ \quad + \cos(a - \pi/2) + \sin(a) \\ y = \sin(-s + a + \pi/2 + (a + c \cos[a])) + \\ \quad \tan(a)(c \cos(a)) + \sin(a - \pi/2) + 1 - \cos(a) \end{cases} \quad (17)$$

where $s \in \{a + c \cos(a), b + a + c \cos(a)\}$, and b is the length of the second arc, or the angle formed by this arc.

Thus to find the Dubins path of type LSR between the origin and any given final position and orientation, it is sufficient to solve for the values of parameters a , b , and c . Let (x_f, y_f, ψ_f) denote the coordinates and orientation of the final position. In an LSR configuration the value of the final orientation will be equal to the angle

of the first arc (a) subtracted from the second one (b). Thus the values of a , b , and c are obtained by solving the following system of equations:

$$\begin{cases} x_f = \cos(-s + a + \pi/2 + (a + c \cos(a))) + c \cos(a) \\ \quad + \cos(a - \pi/2) + \sin(a) \\ y_f = \sin(-s + a + \pi/2 + (a + c \cos(a))) + \tan(a)(c \cos(a)) \\ \quad + \sin(a - \pi/2) + 1 - \cos(a) \\ \psi_f = a - b \end{cases} \quad (18)$$

4.2 3D Path Planning

The extension of the 2D Dubins problem into 3D space is not a trivial task, also considering dynamical constraints could add up more complexity. Sussman [21] used optimal control on manifolds to prove that a minimal path could be either a helicoidal arc, or arcs of the form C, S, CS, CSC, CCC. A special case where the initial and terminal vectors belongs to the one plane, can be easily figured out to be a 2D Dubins path lying in the considered plane. In the method described below we present an approach to generate sub-optimal yet efficient trajectories that links two skew vectors, by using two planar dubins paths in two different planes.

In the inertial frame (o, x, y, z) , the generalized coordinates sufficient to describe the vehicle's motion are given as (x, y, z, ψ, θ) . The initial configuration is considered as a unit vector V_0 at point o directed along the (o, x) axis, whereas the final configuration is considered as a unit vector V_f at a point $P_f = (x_f, y_f, z_f)$, with a final yaw angle ψ_f , and a final pitch angle θ_f . The final configuration is then expressed as $C_f = (P_f, \theta_f, \psi_f)$. Our approach for path planning in 3D is based upon finding two planar Dubins paths Γ_h and Γ_v , where Γ_h lies in the horizontal plane (x, o, y) , and Γ_v lies in the vertical plane (x, o, z) , refer to Fig. 4.2. The horizontal Dubins path Γ_h is generated using the method described above, where the initial position is always taken as the origin and the projection of V_f on plane (x, o, y) as the final position.

Whereas the vertical path Γ_v , viewed in plane (x, o, z) , is generated similarly by taking the projection of the final position onto the considered plane. Thus the 3D path is obtained by the intersection of the extrusions of curves Γ_h and Γ_v , as viewed in Fig. 4.2.

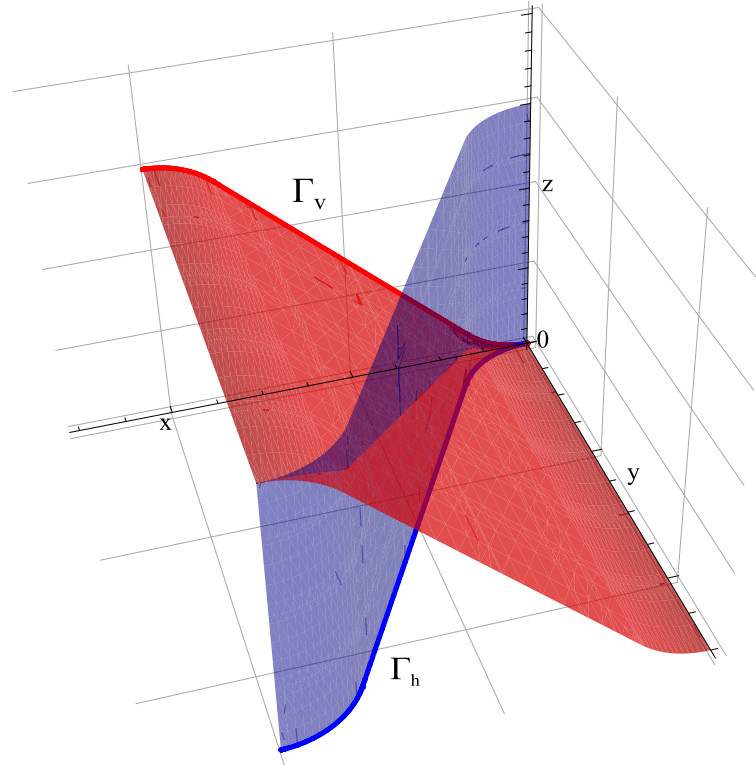


Figure 4.2: Horizontal (blue) and vertical (red) path projections

Three types of subpaths, P_1 , P_2 , and P_3 , are distinguished.

1. The subpath P_1 is the case where the horizontal and vertical projections are two arcs of circles, thus P_1 could be described as a curve resulting from an intersection of two cylinders.
2. The subpath P_2 appears when one of the paths becomes a straight line while the other path is still an arc of a circle. This subpath can be obtained by the intersection of a cylinder and an inclined plane.
3. The third subpath P_3 is a straight line generated by the intersection of two

inclined planes, where the first plane passes through the straight line segment of the horizontal path projection Γ_h , and the second plane passes through the straight line segment of the vertical projection Γ_v .

Fig. 4.3 show the three subpaths P_1 , P_2 , and P_3 , respectively.

The complete path Γ generated would be then a concatenation of 5 subpaths maximum, selected from P_1 , P_2 , and P_3 in the following order:

$$P_{1,1} \rightarrow \begin{pmatrix} P_{2,1} \\ or \\ P_{2,2} \end{pmatrix} \rightarrow P_3 \rightarrow \begin{pmatrix} P_{2,2} \\ or \\ P_{2,1} \end{pmatrix} \rightarrow P_{1,2}$$

The formulation of the path generating algorithm would take the following form:

1. The initial subpath $P_{1,1}$ is always an intersection of two cylinders, starting from the origin point. The curve is plotted as the parameter $s \in \{0, a_{min}\}$, where $a_{min} = \min(a_h, a_v)$ is the minimum arc length between the horizontal and the vertical Dubins curves a_h and a_v respectively.
2. The second subpath $P_{2,1}$ is plotted as $s \in \{a_{min}, a_{max}\}$, where $a_{max} = \max(a_h, a_v)$. Note that the subpaths of type P_2 could take two forms: (i) intersection of a cylinder passing through the circular subpath of Γ_h (normal to the horizontal plane) and an inclined plane passing through the straight line segment of Γ_v , in the case where $a_h > a_v$. (ii) intersection of a cylinder passing through the circular subpath of Γ_v (normal to the vertical plane) and an inclined plane passing through the straight line segment of Γ_h , in the case where $a_v > a_h$.
3. The third subpath P_3 is the straight line segment of the path, generated as the parameter $s \in \{a_{max}, a_{max} + c \cos[a_{max}]\}$, where $c = c_h$ if $a_h > a_v$, or $c = c_v$ if $a_v > a_h$.

4. Similar to $P_{2,1}$, the subpath $P_{2,2}$ could take two forms depending on the values of parameters b_h and b_v . $P_{2,2}$ is plotted as $s \in \{c \cos[a_{max}] + b, c \cos[a_{max}] + a_{max} + d\}$, where $d = b_h - b_v$ if $b_h > b_v$, or $d = b_v - b_h$ if $b_v > b_h$.
5. Subpath $P_{1,2}$ is the last piece of the complete path, which is generated as an intersection of two cylinders, with $s \in \{c \cos[a_{max}] + b + d, c \cos(a_{max}) + a_{max} + d + e\}$, where $e = \min(b_h, b_v)$.

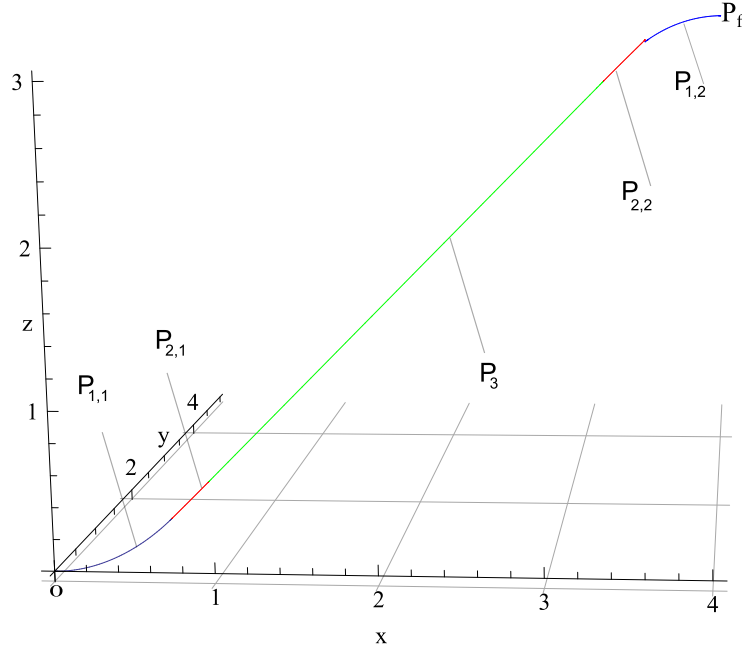


Figure 4.3: Example of a 3D generated path

4.3 Projecting from Different Vertical Planes

In the method described above, the 3D path was generated using the extrusions of a horizontal dubins path in plane (x, o, y) and a vertical one in plane (x, o, z) . Here we try to extend this method by constructing the vertical dubins path in planes different than (x, o, z) . Lets define a plane Π to be perpendicular to the horizontal plane (x, o, y) , passing through the vertical axis (o, z) , and making an angle α with the plane (x, o, z) . The pitch rotation is viewed about a vector normal to this plane. A vertical Dubins path $\Gamma_{v,p}$ is traced in the plane Π by using the projections of

the final position onto the considered plane. Let (x_p, z_p) denote the coordinates of

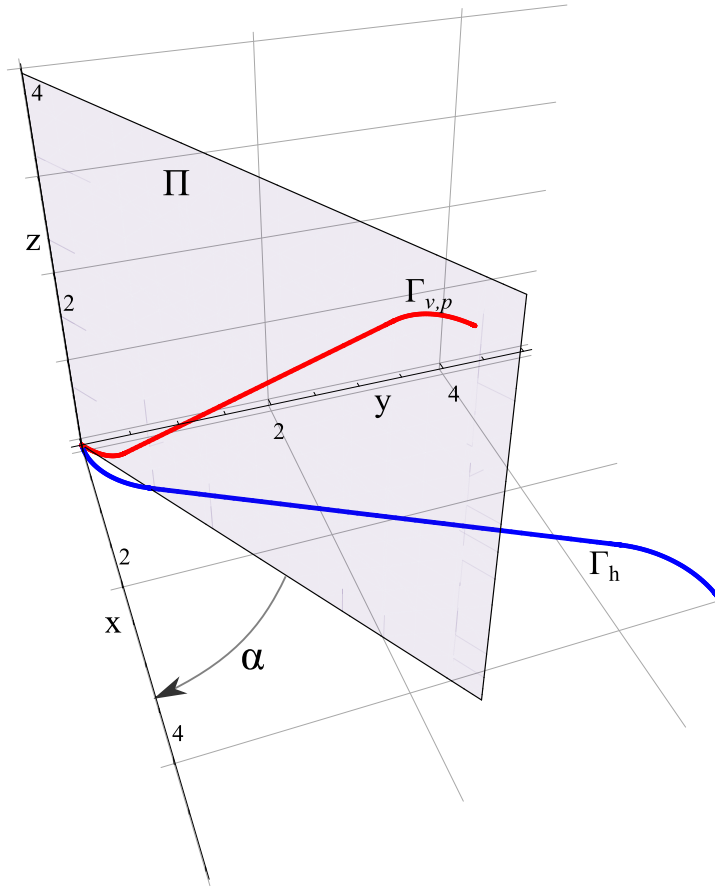


Figure 4.4: Horizontal and Vertical Paths with Plane Π

the projection of the final position onto plane Π , $\theta_{f,p}$ denotes the projection of the final pitch angle, and $V_{f,p}$ be the projection of V_f . These projected parameters are expressed in terms of the final position and orientation as the following:

$$x_p = \sqrt{x_f^2 + y_f^2} \cos\left(\tan^{-1}(x_f, y_f) - \alpha\right), \quad z_p = z_f,$$

$$\theta_{f,p} = \tan^{-1}(\cos(\theta_f) \cos(\psi_f - \alpha), \sin(\theta_f));$$

The 3D curve is constructed in the same fashion as the original method described above, by finding the intersection of the extrusions of the horizontal and vertical curves. Thus by varying the angle α in a bounded range $[\alpha_1, \alpha_2]$, different 3D curves are obtained. Therefore, the shortest path is to be chosen amongst the set

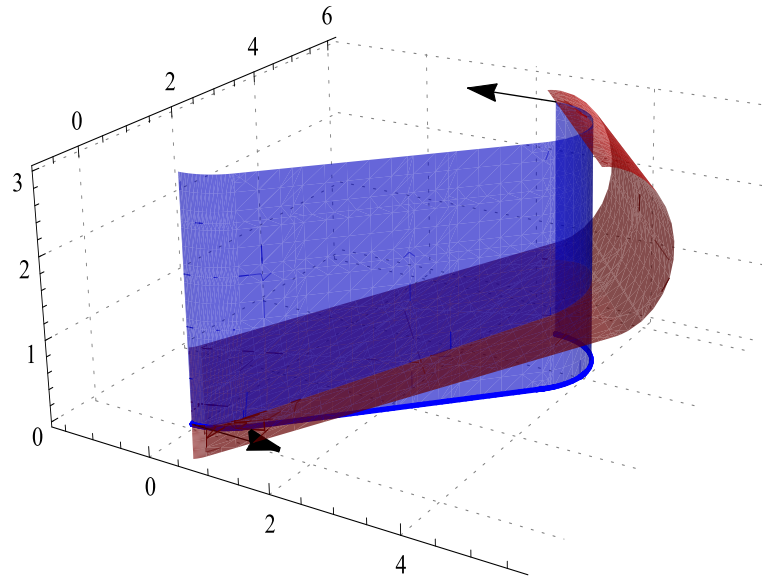
of feasible paths produced by this formulation. Not every value of $\alpha \in]-\frac{\pi}{2}, \frac{\pi}{2}[$ can produce a feasible solution for a 3D path; there exist cases where a vertical Dubins path cannot be constructed when the projection of the final configuration vector V_f onto plane $\mathbf{\Pi}$ becomes a point. Specifically, the range of α is dependent to the final configuration C_f , and could be determined separately for each case subject to the following conditions:

- The projection of the initial or final vector on plane $\mathbf{\Pi}$ should not be a point, or in other words the initial or terminal vectors cannot be normal to plane $\mathbf{\Pi}$.
- The projected final vector $V_{f,p}$ should always be of a positive heading, or the dot product $(o, x_p) \cdot V_{f,p} > 0$.
- The value of the x component of the projected final position x_p should always be greater than $2R$ ($|x_p| > 2R$).

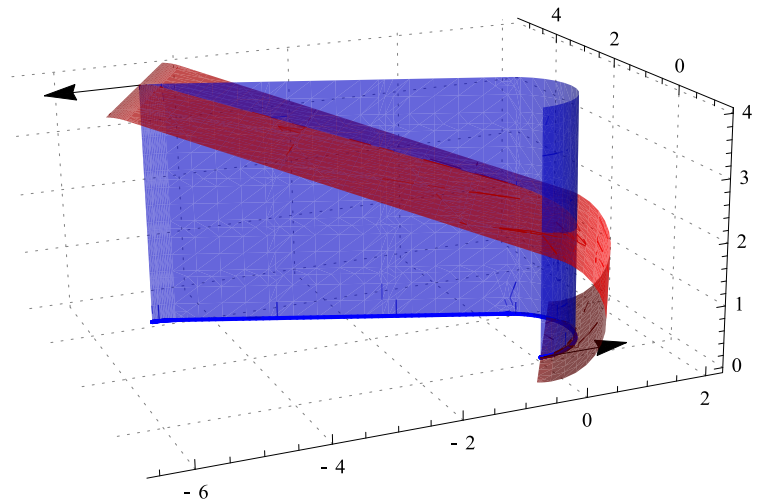
By using this method for 3D path generation, a geometric constraint limiting the range of the final configuration is to be noted. Not every configuration (P_f, ψ_f, θ_f) such that $\{P_f \in \mathbb{R}^3; \psi_f, \theta_f \in [-\frac{\pi}{2}, \frac{\pi}{2}]\}$ could be reached by imposing the described above. The final position should always be ahead of the initial position with a direction pointing forward ($x_f > 0$), and $\psi_f \in [-\frac{\pi}{2}, \frac{\pi}{2}]$. Configurations not satisfying this condition will lead to cases where there is no intersection between the projections of the horizontal and vertical paths.

4.4 3D Path Planning by Unfolding Dubins Surfaces

To cope with these constraints we devise a new path planning technique based also on the Dubins method which could extend the reachable space obtained by the above described methods. In this method we consider the pitch rotation to be about the robot's y-axis. We define a Dubins surface to be the extrusion of a planar



(a) Case where $\psi_f \notin [-\frac{\pi}{2}, \frac{\pi}{2}]$



(b) Case where $x_f < 0$

Figure 4.5: Example of Non-Intersecting Horizontal and Vertical Paths Extrusions

Dubins path, normal to the plane on which the path is drawn in. The 3D path planning follows the following formulation. Given any final configuration (P_f, ψ_f, θ_f) , a horizontal Dubins path Γ_h is constructed using the parameters (x_f, y_f, ψ_f) . This path is then extruded to a height z_f normal to plane (x, o, y) creating, as previously defined, a Dubins surface. Then, the circular edges of this surface are unfolded to form a planar surface of a length equivalent to the length of the horizontal path and a height equal to z_f . A vertical Dubins path is drawn in the unfolded plane using the final parameters (l_h, z_f, θ_f) , where l_h is the length of the horizontal Dubins path, which is considered to be the x-component of the final position. The 3D path is thus obtained by folding back the edges of the considered plane, retaining the original shape of the vertical Dubins surface.

In addition to straight lines (S) and circles (C), two other forms of 3D curves are distinguished:

1. Curve H_1 : a helix with a constant torsion.
2. Curve H_2 : a helix with a circular torsion.

The full path can be broke down into 5 subpaths maximum, having the following order:

$$H_2 \rightarrow \begin{pmatrix} H_1 \\ or \\ C \end{pmatrix} \rightarrow S \rightarrow \begin{pmatrix} C \\ or \\ H_1 \end{pmatrix} \rightarrow H_2$$

- Curve H_2 is determined by wrapping a circle C (or an arc of a circle) isometrically around a cylinder P . Let both the circle and cylinder be of unit radii, and the axis of the cylinder be the z -axis. The circle C lies in a (s, z) -plane witch is determined by the parametric equation $(s, z) = (\cos t, \sin t)$. Cylinder P lies in the coordinate system (x, y, z) with parametric terms $(\cos \psi, \sin \psi, z)$. The wrapping of C around P is a mapping of points (s, z) onto the coordinate system points (x, y, z) with the same z coordinate, where $s = \psi$. Thus the para-

metric representation of curve H_2 is determined as $(x, y, z) = (\cos s, \sin s, z) = (\cos(\cos t), \sin(\cos t), \sin t)$.

- The second curve H_1 is determined in the same fashion as H_2 by wrapping a straight line L about a cylinder P . Let L be a straight line defined in a plane (s, z) determined by the parametric equation $(s, z) = (t, ct)$, where c is the slope of L . Cylinder P is the same as described above. Thus H_1 is determined as the mapping from (s, z) onto (x, y, z) represented parametrically as $(x, y, z) = (\cos s, \sin s, z) = (\cos(t), \sin(t), ct)$.
- Curve C is simply an arc of a circle and would appear in cases where the length of the first arc of the vertical Dubins curve is larger than that of the horizontal curve.
- Curve S is a straight line which is obtained when both the vertical and horizontal Dubins curves are in the form of a straight line.

The complete parametric formulation of the curves is found in the appendix. The figures below show several examples of the path planning method described.

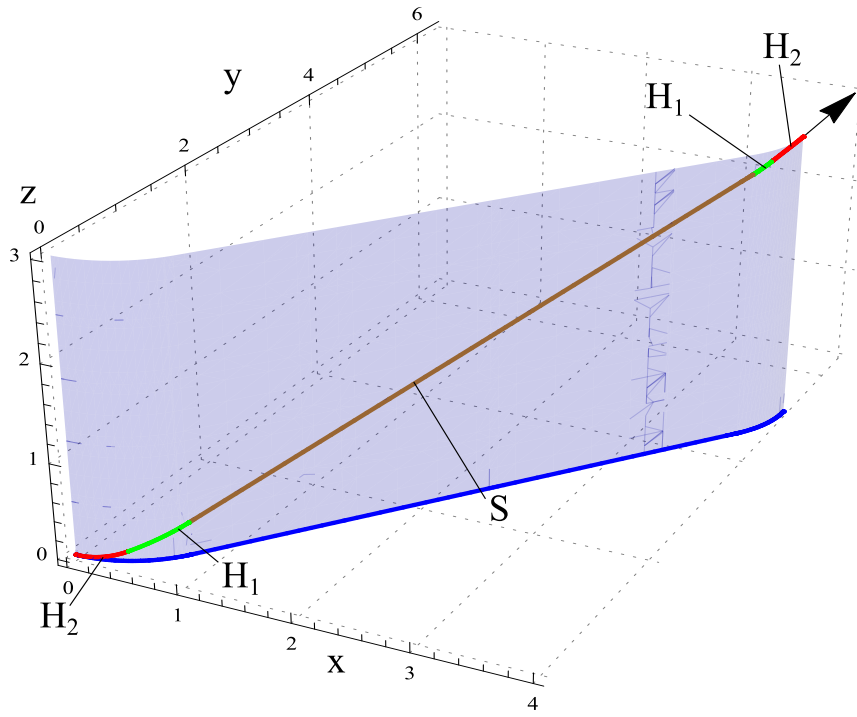


Figure 4.6: 3D Path Example ($x = 4, y = 5, z = 3, \psi = 90 \text{ deg}, \theta = 0 \text{ deg}$)

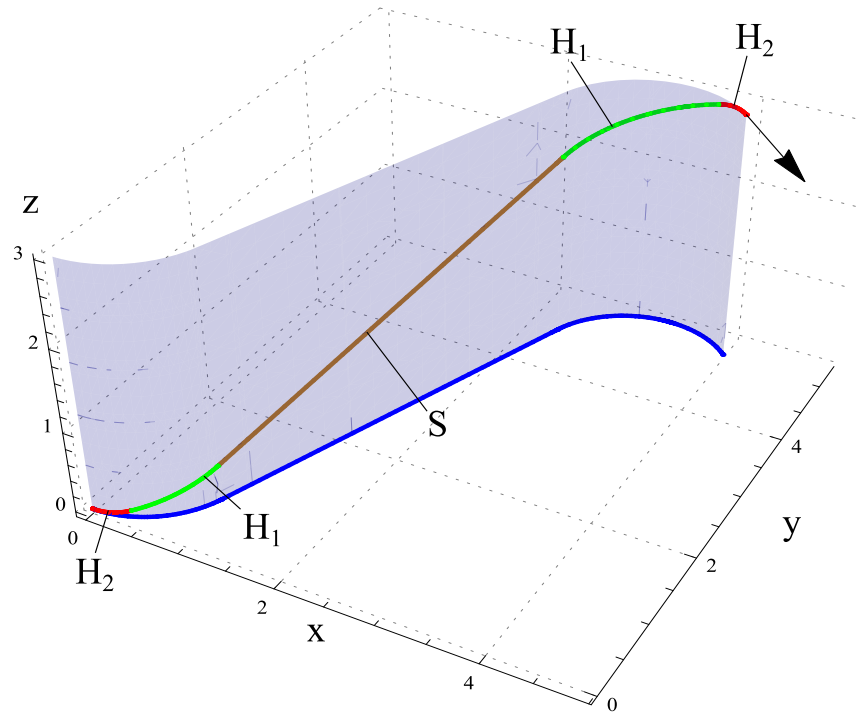


Figure 4.7: 3D Path Example ($x = 4, y = 5, z = 3, \psi = -45 \text{ deg}, \theta = 0 \text{ deg}$)

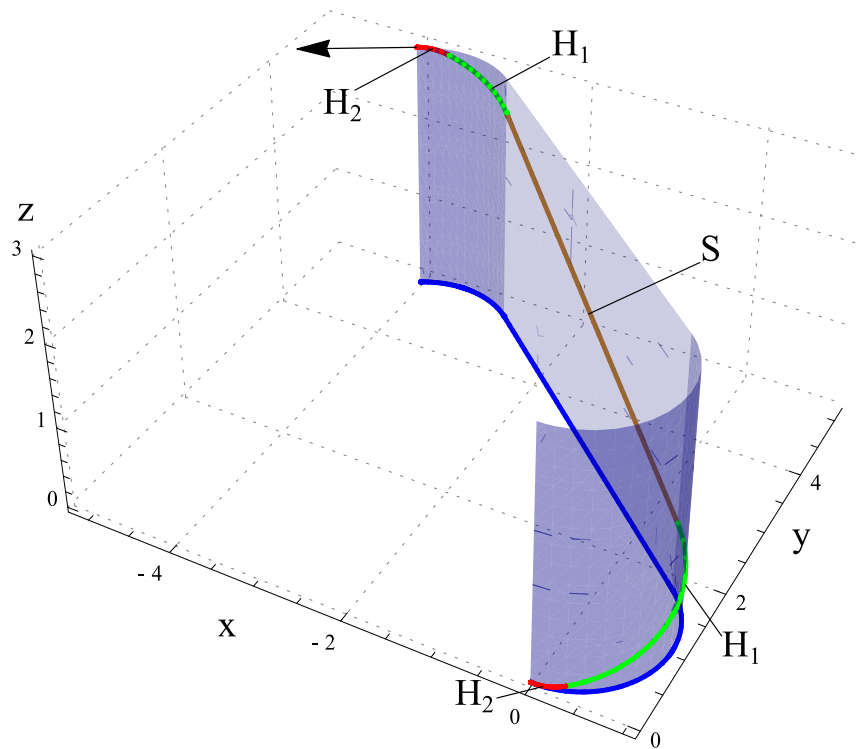


Figure 4.8: 3D Path Example ($x = -4, y = 5, z = 3, \psi = 210 \text{ deg}, \theta = 0 \text{ deg}$)

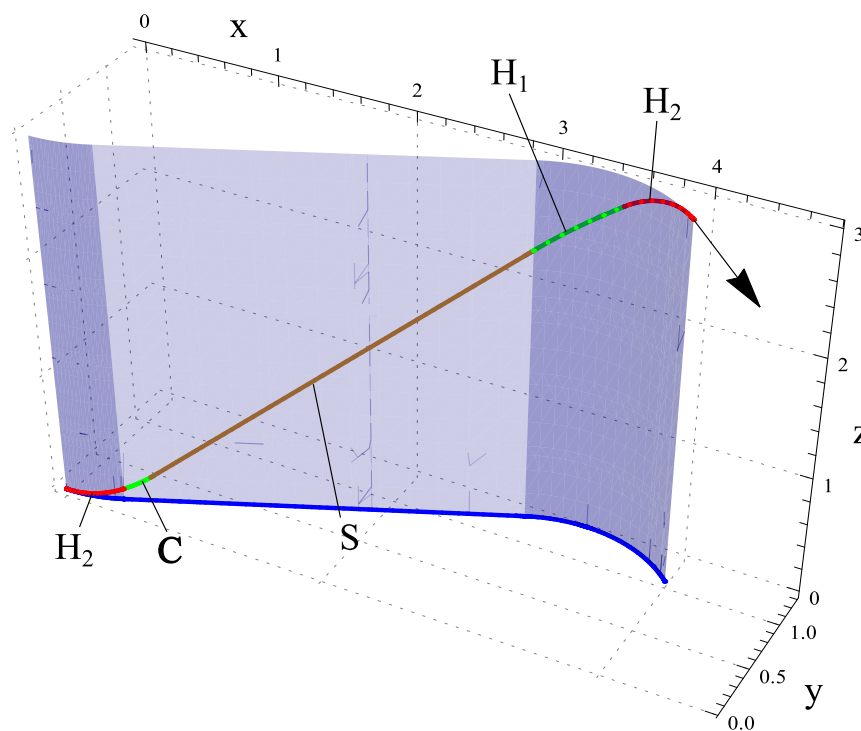


Figure 4.9: 3D Path Example ($x = 4, y = 1, z = 3, \psi = -45 \text{ deg}, \theta = 0 \text{ deg}$)

4.5 Motion Constraints

One of the major dynamic constraints for an underwater vehicle maneuvering in a 3D space is the vertical maximum climbing (or diving) angle α_{max} , which is limited due to the action of the control actuators. The climbing angle describes the rate of change of altitude (z), which should not be confused with the pitch angle θ . In our case, we always consider that the heading vector of the robot is always moving tangent to the path considered, which allow us to assume the coincidence of the climbing and the pitch angles ($\alpha = \theta$). The parametric form of the climb angle is expressed as:

$$\theta(t) = \tan^{-1} \left(\frac{\dot{z}(t)}{\sqrt{\dot{x}(t)^2 + \dot{y}(t)^2}} \right) \quad (19)$$

Thus for climb and dive maximum angles, the absolute maximum values are described as $|\theta(t)| < \theta_{max}$, where θ_{max} (maximum pitch angle) is to be computed experimentally. This constraint significantly leads us to distinguish two cases in our path planning method. A low altitude configuration where the altitude of the goal position lies beneath the value allowed by the maximum pitch angle constraint, and a high altitude configuration where the vehicle cannot reach its goal destination using the method described above, due to this maximum pitch angle constraint. Thus another method is to be devised.

4.6 High Altitude Configuration

In this case, in order to overcome the constraint discussed above, we consider the same kind of path described above but combined with a helical path on the top of it. The key point here is to keep a maximum value of the pitch angle θ as much as possible through out the whole trajectory and switching to the desired pitch angle value right before reaching the goal destination. A path is traced using the horizontal Dubin projection Γ_h along with the pitch angle θ driven to its maximum

θ_{max} . When the final horizontal position (x_f, y_f, θ_h) is reached, keep adding circles with minimum radius and maximum pitch until the final altitude z_f is reached. Fig. 4.10 shows an example of a high altitude configuration, where the vehicle would trace a helix for two turns then switches to its desired orientation as its reaches its final position.

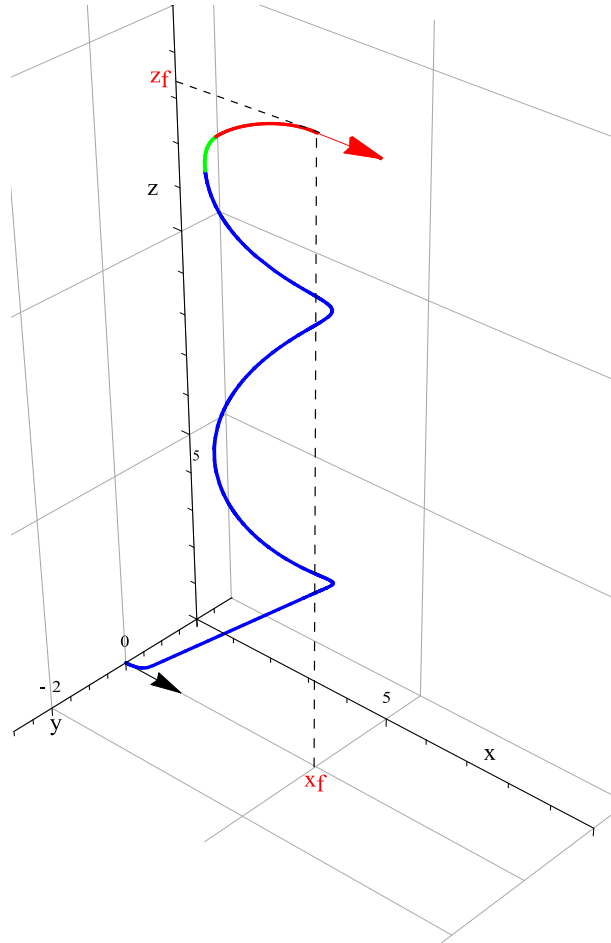


Figure 4.10: Example of a High Altitude path

Therefore as Dubins curves could be solved for any 2 points in a plane, our method provides a solution for a minimal length curves given any 2 points in a 3D space.

4.7 Discussion of Different Path Planning Methods

Path planning methods described in Chitsaz and LaValle [6] and Pachikara et al. [20] described the kinematic model of an airplane or any body maneuvering in a 3D environment to be a 4-state system (x, y, z, ψ) and thus neglecting any pitch rotation. Such models could maybe used to describe the motion of vehicles with vertical thrusters such as helicopters for example. But for systems such as underwater vehicles or airplanes which are provided with a horizontal thruster and control fins to steer themselves, a 4-state kinematic model would be insufficient to describe their motion since such systems require to change their pitch angle in order to change their altitude. The 3D path planning methods described in this thesis account for the additional pitch rotation and extend the model into a 5-state system (x, y, z, ψ, θ) .

On the other hand, if we consider a case where the initial and final vectors lie in two parallel planes having both a zero pitch angle. Then the total length of a path generated by methods described by Chitsaz and LaValle [6] or Pachikara et al. [20] would be shorter than the length of a path generated by our method since the vertical motion would be of a constant pitch for a 4-state system rather than our Dubins type motion for a 5-state system. But driving a body with a geometry similar to that of an underwater vehicle or an airplane, along a path provided by Chitsaz and LaValle [6] or Pachikara et al. [20] would experience much more resistance since its altitude will change without changing its pitch. It is clear that such a path will produce much larger resistive forces on the UAV since it is traveling along a path that does not minimize its effective cross-sectional areas. In our approach, even though, the length of the path is relatively longer, however, we believe that our overall energetic cost is smaller simply due to the fact that we enforce that the vehicle is always tangent to the proposed path and thus minimizing the drag forces.

CHAPTER 5

CONCLUSIONS

In this work we have provided a brief description of a conceptual mechanical design of a hybrid autonomous underwater vehicle. We derived the complete kinematic and dynamic modeling of the system and provided some open loop simulation. We have proposed a 3D path generating algorithm using two planar Dubins curves as the horizontal and vertical projection of the full path. Knowing the fact that the Dubins curves are optimal within a plane, allows us to assume a sub-optimality of the path generated. Our future work involve a further study of the optimality of the paths generated and comparing our method to the work done by Sussman [21] on 3-d paths with prescribed curvature bound, and to other similar path planning techniques. It will also be interesting to introduce the constraint on the climbing angle and formulate it with the Pontryagin's Maximal Principal (PMP) [6] to compute truly optimal paths. The last part of our work would be implementing our results on a actual platform.

CHAPTER 6

APPENDIX

- Rigid Body Inertia Matrix:

$$M_{RB} = \begin{pmatrix} mI_{3 \times 3} & -mS(r_G) \\ mS(r_G) & I_0 \end{pmatrix}$$
$$M_{RB} = \begin{pmatrix} m & 0 & 0 & 0 & mz_G & 0 \\ 0 & m & 0 & -mz_G & 0 & mx_G \\ 0 & 0 & m & 0 & -mx_G & 0 \\ 0 & -mz_G & 0 & I_x & 0 & -I_{xz} \\ mz_G & 0 & -mx_G & 0 & I_y & 0 \\ 0 & mx_G & 0 & -I_{xz} & 0 & I_z \end{pmatrix}$$

- Rigid Body Coriolis and Centripetal Matrix:

$$C_{RB}(\nu) = \begin{pmatrix} 0 & 0 & 0 & c_{41} & -c_{51} & -c_{61} \\ 0 & 0 & 0 & -c_{42} & c_{52} & -c_{62} \\ 0 & 0 & 0 & -c_{43} & -c_{53} & c_{63} \\ -c_{41} & c_{42} & c_{43} & 0 & -c_{54} & -c_{64} \\ c_{51} & -c_{52} & c_{53} & c_{54} & 0 & c_{65} \\ c_{61} & c_{62} & -c_{63} & c_{64} & c_{65} & 0 \end{pmatrix}$$

where,

$$\begin{aligned}
c_{41} &= mz_{Gr}; & c_{42} &= mw; \\
c_{43} &= m(z_{Gp} - v); \\
c_{51} &= m(x_{Gq} - w); & c_{52} &= m(z_{Gr} + x_{Gp}); \\
c_{53} &= m(z_{Gq} + u); & c_{54} &= I_{zx}p - I_zr; \\
c_{61} &= m(x_{Gr} + v); & c_{62} &= -mu; \\
c_{63} &= mx_{Gr}; & c_{64} &= I_yq; \\
c_{65} &= I_{zx}r - I_xp;
\end{aligned}$$

- Added Mass Inertia Matrix:

$$M_A = - \begin{pmatrix} X_{\dot{u}} & 0 & 0 & 0 & 0 & 0 \\ 0 & Y_{\dot{v}} & 0 & 0 & 0 & N_{\dot{v}} \\ 0 & 0 & Z_{\dot{w}} & 0 & Z_{\dot{q}} & 0 \\ 0 & 0 & 0 & K_{\dot{p}} & 0 & 0 \\ 0 & 0 & M_{\dot{u}} & 0 & M_{\dot{q}} & 0 \\ 0 & Y_{\dot{r}} & 0 & 0 & 0 & N_{\dot{r}} \end{pmatrix}$$

- Added Mass Coriolis and Centripetal Matrix:

$$C_A(\nu) = \begin{pmatrix} 0 & 0 & 0 & \dots \\ 0 & 0 & 0 & \dots \\ 0 & 0 & 0 & \dots \\ 0 & -Z_{\dot{w}}w - M_{\dot{w}}q & Y_{\dot{v}}v + N_{\dot{v}}v & \dots \\ Z_{\dot{w}}w + M_{\dot{w}}q & 0 & -X_{\dot{u}}u & \dots \\ -Y_{\dot{v}}v - N_{\dot{v}}v & X_{\dot{u}}u & 0 & \dots \\ \dots & 0 & -Z_{\dot{w}}w - M_{\dot{w}}q & Y_{\dot{v}}v + N_{\dot{v}}v \\ \dots & Z_{\dot{w}}w + M_{\dot{w}}q & 0 & -X_{\dot{u}}u \\ \dots & -Y_{\dot{v}}v - N_{\dot{v}}v & X_{\dot{u}}u & 0 \\ \dots & 0 & -N_{\dot{v}}v - N_{\dot{r}}r & M_{\dot{w}}w + M_{\dot{q}}q \\ \dots & N_{\dot{v}}v + N_{\dot{r}}r & 0 & -K_{\dot{p}}p \\ \dots & -M_{\dot{w}}w - M_{\dot{q}}q & K_{\dot{p}}p & 0 \end{pmatrix}$$

- Crossflow Added Mass Coefficients:

$$Y_{\dot{v}} = Z_{\dot{w}} = - \int_{x-tail}^{x-nose} \rho \pi a^2 dx$$

$$M_{\dot{q}} = N_{\dot{r}} = - \int_{x-tail}^{x-nose} x^2 \rho \pi a^2 dx$$

$$M_{\dot{w}} = -N_{\dot{v}} = - \int_{x-tail}^{x-nose} x \rho \pi a^2 dx$$

- Crossflow Drag:

$$\begin{aligned}
Y_{v|v} = Z_{w|w} &= -\frac{1}{2}\rho c_{dc} \int_{x-tail}^{x-nose} 2R(x)dx - 2 \left(\frac{1}{2}\rho S_{fin} c_{df} \right) \\
M_{w|w} = -N_{v|v} &= -\frac{1}{2}\rho c_{dc} \int_{x-tail}^{x-nose} 2xR(x)dx - 2x_{fin} \left(\frac{1}{2}\rho S_{fin} c_{df} \right) \\
Y_{r|r} = -Z_{q|q} &= -\frac{1}{2}\rho c_{dc} \int_{x-tail}^{x-nose} 2x|x|R(x)dx - 2x_{fin}|x_{fin}| \left(\frac{1}{2}\rho S_{fin} c_{df} \right) \\
M_{q|q} = N_{r|r} &= -\frac{1}{2}\rho c_{dc} \int_{x-tail}^{x-nose} 2x^3R(x)dx - 2x_{fin}^3 \left(\frac{1}{2}\rho S_{fin} c_{df} \right)
\end{aligned}$$

where c_{dc} is the drag coefficient of a cylinder, $R(x)$ is the hull radius as a function of axial, S_{fin} is the control fin plan form area, and c_{df} is the crossflow drag coefficient of the control fins.

- Rolling Drag:

$$K_{p|p} = Y_{vvf} r_{mean}^3$$

where Y_{vvf} is the fin component of the vehicle crossflow drag coefficient, and r_{mean} is the mean fin height above the vehicle centerline.

- Body Lift Coefficients:

$$\begin{aligned}
Y_{wvl} = Z_{uwl} &= -\frac{1}{2}\rho A_p c_{yd\beta} \\
M_{uwl} = N_{wvl} &= -\frac{1}{2}\rho A_p c_{yd\beta} x_{cp}
\end{aligned}$$

where A_p is the projected area of the vehicle hull, $c_{yd\beta}$ is the body lift coefficient, and x_{cp} is the position of the vehicle's center of pressure.

- Fin Lift Coefficients:

$$\begin{aligned}
Y_{uu\delta r} &= \frac{1}{2}\rho A_p c_{L\alpha} S_{fin} \\
Z_{uu\delta s} &= -\frac{1}{2}\rho A_p c_{L\alpha} S_{fin} \\
M_{uu\delta s} &= \frac{1}{2}\rho A_p c_{L\alpha} S_{fin} x_{fin} \\
M_{uu\delta r} &= \frac{1}{2}\rho A_p c_{L\alpha} S_{fin} x_{fin}
\end{aligned}$$

- 3D Paths by Unfolding Dubins Surfaces parametric equations.

Let (a_h, b_h, c_h) and (a_v, b_v, c_v) be the parameters of the horizontal and vertical Dubins curves respectively, where a is the length of the first arc, b is the length of the second arc, and c is the length of the straight line segment. The parametric equations of a (H_2, H_1, S, H_1, H_2) path are given as:

$$\begin{aligned}
H_2 &: \left(\sin(\cos(t - \frac{\pi}{2})), 1 - \cos(\cos(t - \frac{\pi}{2})), \sin(t - \frac{\pi}{2}) + 1 \right), t \in (0, a_v); \\
H_1 &: \left(\sin(\cos(a_v - \frac{\pi}{2}) + t), 1 - \cos(\cos(a_v - \frac{\pi}{2}) + t), t \tan(a_v) + \sin(a_v - \frac{\pi}{2}) + 1 \right) \\
&, t \in (0, c_1); \\
S &: Rot_{z, a_h} \cdot Rot_{y, a_v} \cdot (t, 0, 0) + \\
&\left(\sin(\cos(a_v - \frac{\pi}{2}) + c_1), 1 - \cos(\cos(a_v - \frac{\pi}{2}) + c_1), c_1 \tan(a_v) + \sin(a_v - \frac{\pi}{2}) + 1 \right) \\
&, t \in (0, \frac{c_h}{\cos(a_v)}); \\
H_1 &: \left(c_h \cos(a_h) + \cos(a_v - t + \frac{\pi}{2}) + \sin(a_h) + \cos(a_h - \frac{\pi}{2}), \tan(a_h)(c_h \cos(a_h)) + \right. \\
&\sin(a_h - t + \frac{\pi}{2}) + \sin(a_h - \frac{\pi}{2}) - \cos(a_h) + 1, c_1 \tan(a_v) + \frac{c_h}{\cos(a_v)} \sin(a_v) + \\
&t \tan(a_v) + \sin(a_v - \frac{\pi}{2}) + 1 \left. \right), t \in (0, c_2); \\
H_2 &: \left(\cos(a_h - b_h + \frac{\pi}{2} - \cos(a_v - t + \frac{\pi}{2})) + c_h \cos(a_h) + \sin(a_h) + \cos(a_h - \frac{\pi}{2}), \right. \\
&\sin(a_h - b_h + \frac{\pi}{2} - \cos(a_v - t + \frac{\pi}{2})) + \tan(a_h)(c_h \cos(a_h)) + \sin(a_h - \frac{\pi}{2}) - \cos(a_h) + 1, \\
&\tan(a_v)(c_v \cos(a_v)) + \sin(a_v - t + \frac{\pi}{2}) + \sin(a_v - \frac{\pi}{2}) - \cos(a_v) + 1 \left. \right), t \in (0, b_v).
\end{aligned}$$

where

$$c1 = a_h - \tan^{-1}(\cos(\sin(a_v v)), \sin(\sin(a_v))),$$

and

$$c2 = a_h - \tan^{-1}(\cos(a_v) \cos(a_h + \sin(a_v v) - b_h), \cos(a_v) \sin(a_h + \sin(a_v) - b_h)).$$

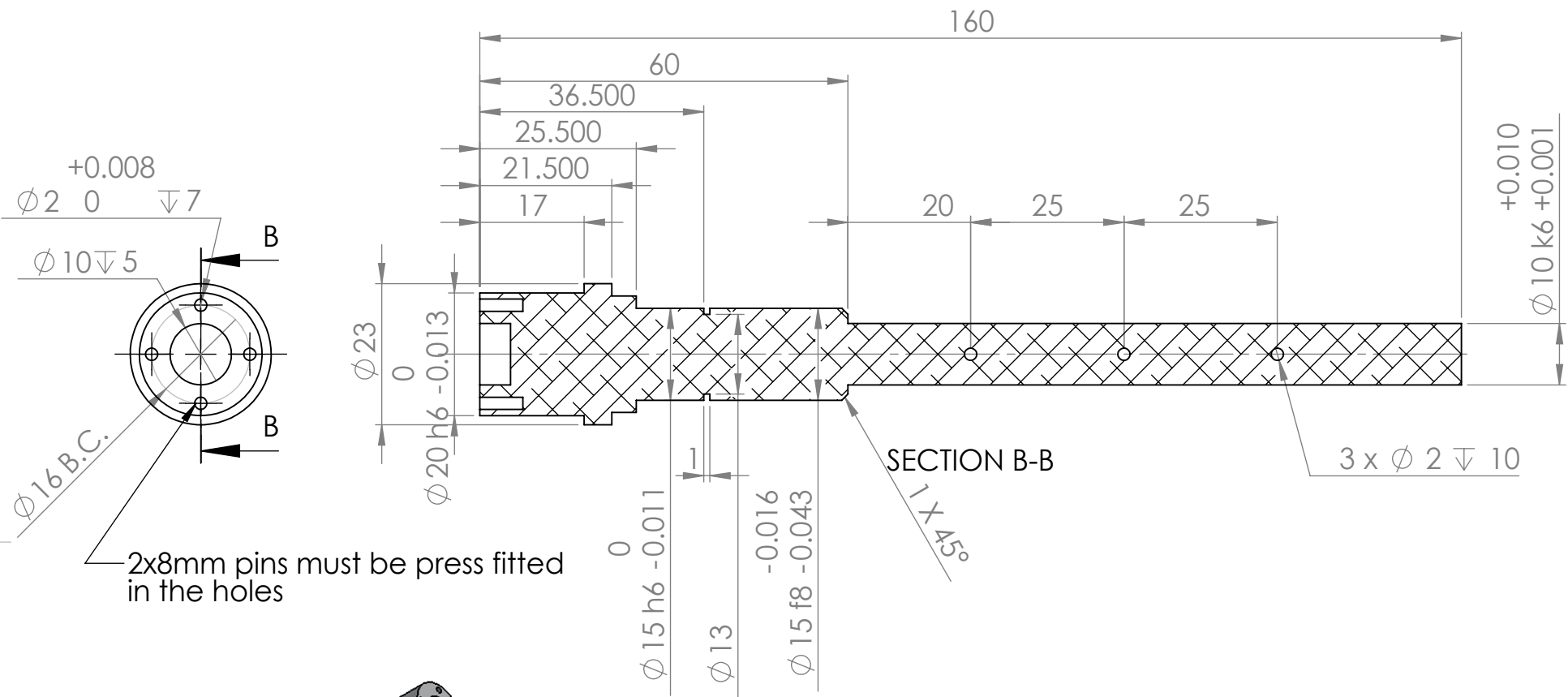
REFERENCES

- [1] Andrea Balluchi, Antonio Bicchi, Aldo Balestrino, and Giuseppe Casalino. Path tracking control for dubin's cars. In *Robotics and Automation, 1996. Proceedings., 1996 IEEE International Conference on*, volume 4, pages 3123–3128. IEEE, 1996.
- [2] JG Bellingham. Platforms: autonomous underwater vehicles. *Encyclopedia of Ocean Sciences*, pages 473–484, 2009.
- [3] JG Bellingham, CA Goudey, TR Consi, JW Bales, DK Atwood, JJ Leonard, and C Chryssostomidis. A second generation survey auv. In *Autonomous Underwater Vehicle Technology, 1994. AUV'94., Proceedings of the 1994 Symposium on*, pages 148–155. IEEE, 1994.
- [4] Robert D Blevins and R Plunkett. Formulas for natural frequency and mode shape. *Journal of Applied Mechanics*, 47:461, 1980.
- [5] Andrea Caiti and Vincenzo Calabro. Control-oriented modelling of a hybrid auv. In *Robotics and Automation (ICRA), 2010 IEEE International Conference on*, pages 5275–5280. IEEE, 2010.
- [6] Hamidreza Chitsaz and Steven M LaValle. Time-optimal paths for a dubins airplane. In *Decision and Control, 2007 46th IEEE Conference on*, pages 2379–2384. IEEE, 2007.
- [7] Russ E Davis, Charles C Eriksen, and Clayton P Jones. Autonomous buoyancy-driven underwater gliders, 2002.
- [8] Lester E Dubins. On curves of minimal length with a constraint on average curvature, and with prescribed initial and terminal positions and tangents.

- American Journal of mathematics*, pages 497–516, 1957.
- [9] Jason Evans and Meyer Nahon. Dynamics modeling and performance evaluation of an autonomous underwater vehicle. *Ocean Engineering*, 31(14):1835–1858, 2004.
- [10] Odd Faltinsen. *Sea loads on ships and offshore structures*, volume 1. Cambridge university press, 1993.
- [11] JP Feldman. State-of-the-art for predicting the hydrodynamic characteristics of submarines. In *Proceedings of the Symposium on Control Theory and Naval Applications*, pages 87–127, 1975.
- [12] Thor I. Fossen. *Guidance and Control of Ocean Vehicles*. Wiley, August 1994.
- [13] Morton Gertler and Grant R Hagen. Standard equations of motion for submarine simulation. Technical report, DTIC Document, 1967.
- [14] Joshua G Graver, Ralf Bachmayer, Naomi Ehrich Leonard, and David M Fratantoni. Underwater glider model parameter identification. In *Proceedings of the 13th International Symposium on Unmanned Untethered Submersible Technology*, 2003.
- [15] Sighard F Hoerner. Fluid-dynamic drag (1965) published by the author. *New York, NY*.
- [16] Sighard F Hoerner and Henry V Borst. Fluid-dynamic lift: Practical information on aerodynamic and hydrodynamic lift. *NASA STI/Recon Technical Report A*, 76:32167, 1975.
- [17] Khalid Isa and Mohd Rizal Arshad. Dynamic modeling and characteristics estimation for usm underwater glider. In *Control and System Graduate Research Colloquium (ICSGRC), 2011 IEEE*, pages 12–17. IEEE, 2011.

- [18] Bong-Huan Jun, Jin-Yeong Park, Fill-Youb Lee, Pan-Mook Lee, Chong-Moo Lee, Kihun Kim, Young-Kon Lim, and Jun-Ho Oh. Development of the auv isimiŽand a free running test in an ocean engineering basin. *Ocean Engineering*, 36(1):2–14, 2009.
- [19] N Mahmoudian, J Geisbert, and C Woolsey. Dynamics and control of underwater gliders i: steady motions. Technical report, Technical Report, Virginia Polytechnic Institute and State University, 2009.
- [20] Abraham J Pachikara, Joseph J Kehoe, and Rick Lind. A path-parameterization approach using trajectory primitives for 3-dimensional motion planning. In *Proceedings of the 2009 AIAA Guidance, Navigation, and Control Conference*, 2009.
- [21] LS Pontryagin, VG Boltyanskii, RV Gamkrelidze, and EF Mishchenko. *The Mathematical Theory of Optimal Processes (Interscience, New York, 1962)*. John Wiley, 1962.
- [22] Timothy Prestero. Development of a six-degree of freedom simulation model for the remus autonomous underwater vehicle. In *OCEANS, 2001. MTS/IEEE Conference and Exhibition*, volume 1, pages 450–455. IEEE, 2001.
- [23] Héctor J Sussmann. Shortest 3-dimensional paths with a prescribed curvature bound. In *Decision and Control, 1995., Proceedings of the 34th IEEE Conference on*, volume 4, pages 3306–3312. IEEE, 1995.
- [24] Christopher von Alt, Ben Allen, Thomas Austin, and Roger Stokey. Remote environmental measuring units. In *Autonomous Underwater Vehicle Technology, 1994. AUV'94., Proceedings of the 1994 Symposium on*, pages 13–19. IEEE, 1994.
- [25] Shu-xin Wang, Xiu-jun Sun, Yan-hui Wang, Jian-guo Wu, and Xiao-ming

- Wang. Dynamic modeling and motion simulation for a winged hybrid-driven underwater glider. *China Ocean Engineering*, 25:97–112, 2011.
- [26] L Folger Whicker and Leo F Fehlner. Free-stream characteristics of a family of low-aspect-ratio, all-movable control surfaces for application to ship design. Technical report, DTIC Document, 1958.



$\phi 2 \begin{smallmatrix} 0 \\ +0.008 \end{smallmatrix} \nabla 7$

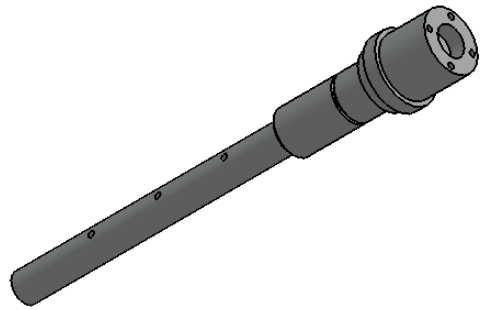
$\phi 10 \nabla 5$

$\phi 16 \text{ B.C.}$

2x8mm pins must be press fitted in the holes

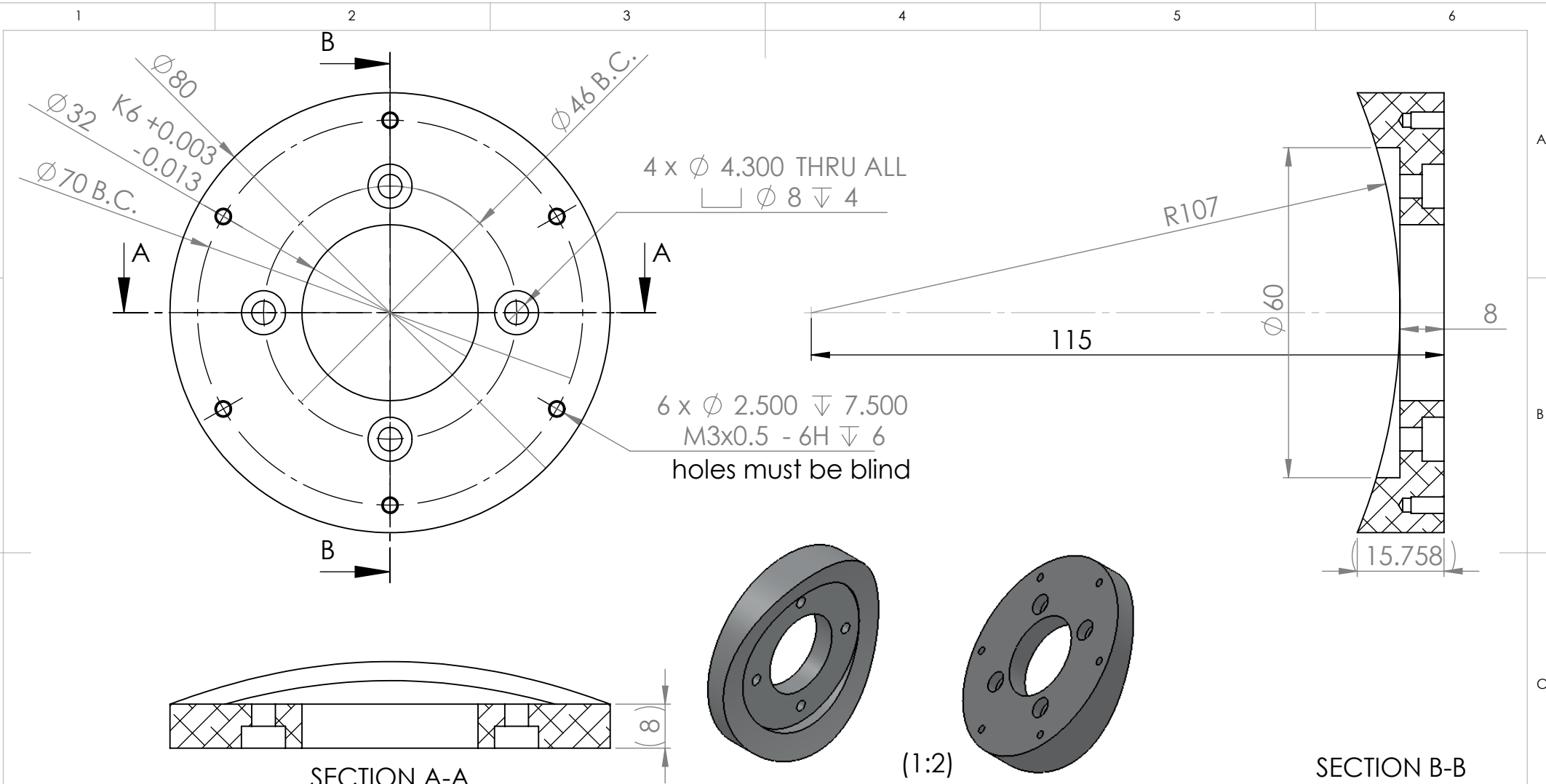
SECTION B-B

3 x $\phi 2 \nabla 10$

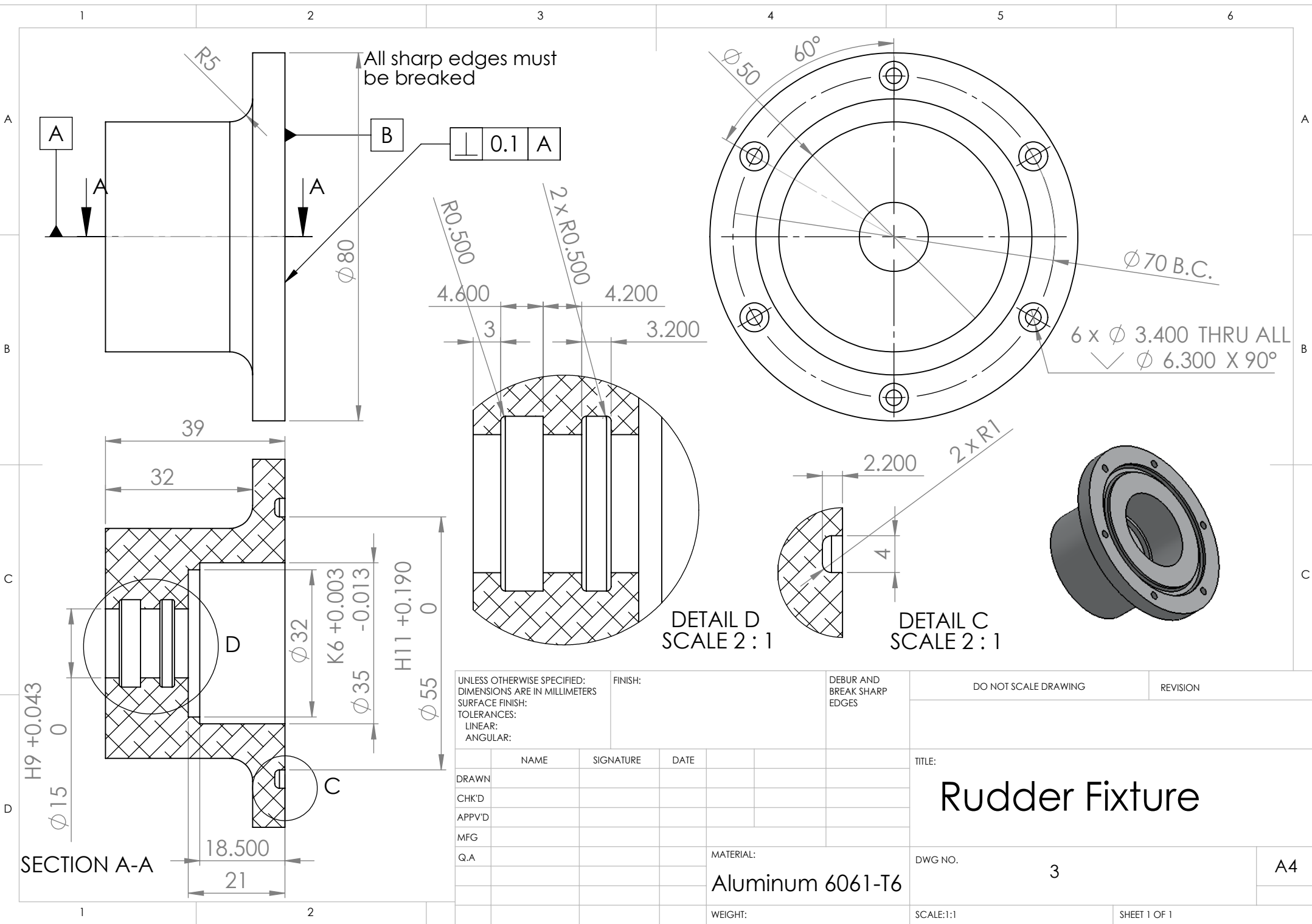


UNLESS OTHERWISE SPECIFIED: DIMENSIONS ARE IN MILLIMETERS SURFACE FINISH: TOLERANCES: LINEAR: ANGULAR:				FINISH:		DEBUR AND BREAK SHARP EDGES		DO NOT SCALE DRAWING		REVISION	
DRAWN				NAME		SIGNATURE		DATE		TITLE:	
CHK'D										<h1>Shaft</h1>	
APPV'D											
MFG											
Q.A											
								MATERIAL: Aluminum 6061-T6		DWG NO. 1	
								WEIGHT:		SCALE:1:1	
										SHEET 2 OF 25	

A4



UNLESS OTHERWISE SPECIFIED: DIMENSIONS ARE IN MILLIMETERS SURFACE FINISH: TOLERANCES: LINEAR: ANGULAR:				FINISH:		DEBUR AND BREAK SHARP EDGES		DO NOT SCALE DRAWING		REVISION	
DRAWN				NAME		SIGNATURE		DATE		TITLE:	
CHK'D										Rudder Fixture Ring	
APPV'D											
MFG											
Q.A											
						MATERIAL:		DWG NO.		A4	
						Aluminum 6061-T6		2			
						WEIGHT:		SCALE:1:1		SHEET 3 OF 25	



UNLESS OTHERWISE SPECIFIED:
 DIMENSIONS ARE IN MILLIMETERS
 SURFACE FINISH:
 TOLERANCES:
 LINEAR:
 ANGULAR:

FINISH:

DEBUR AND
 BREAK SHARP
 EDGES

DO NOT SCALE DRAWING

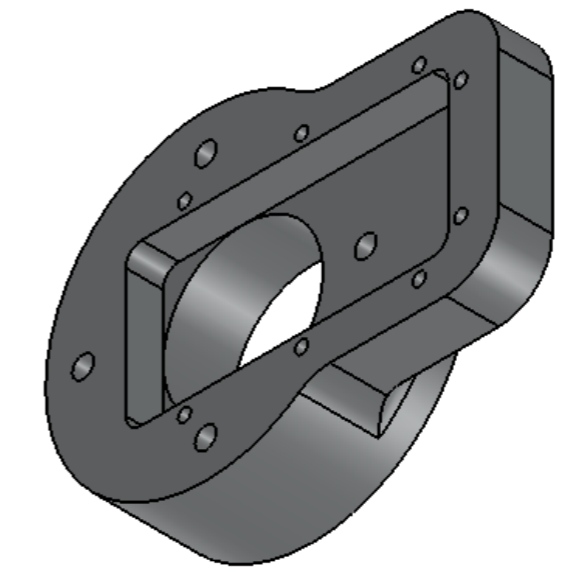
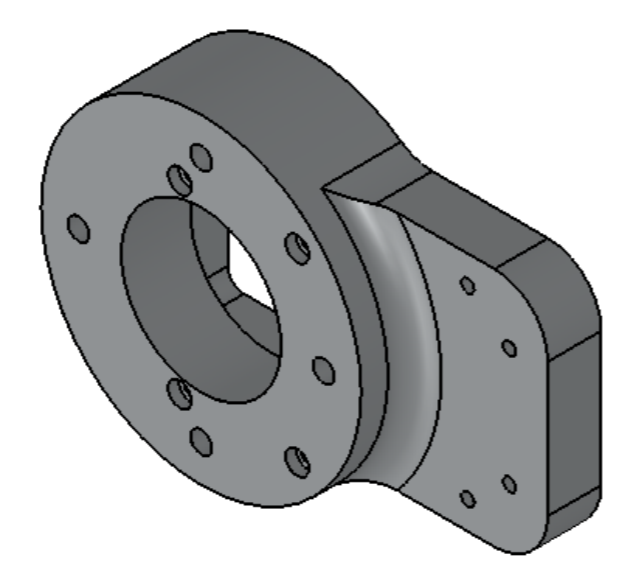
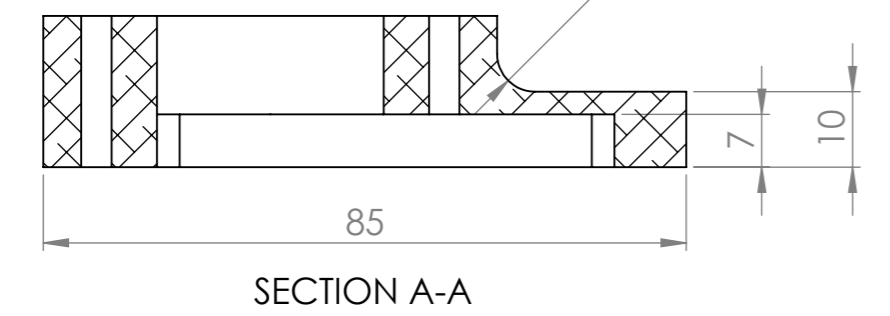
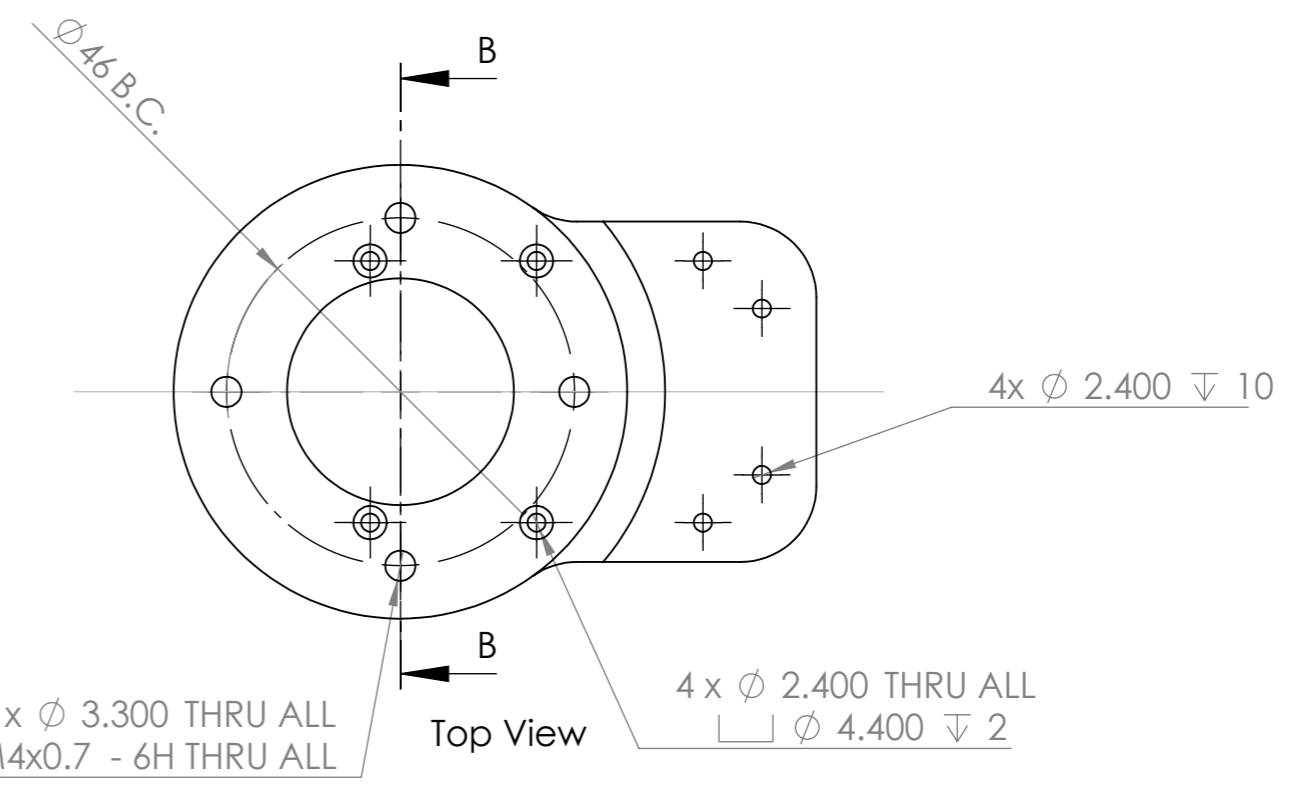
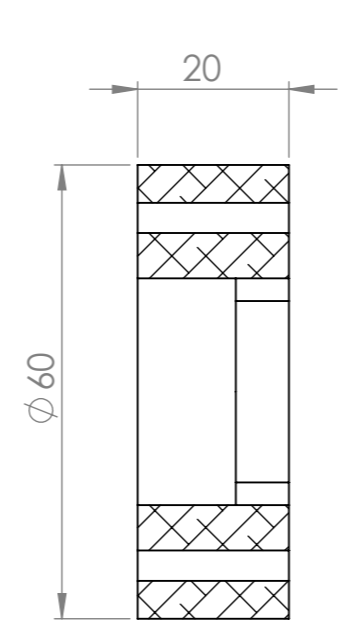
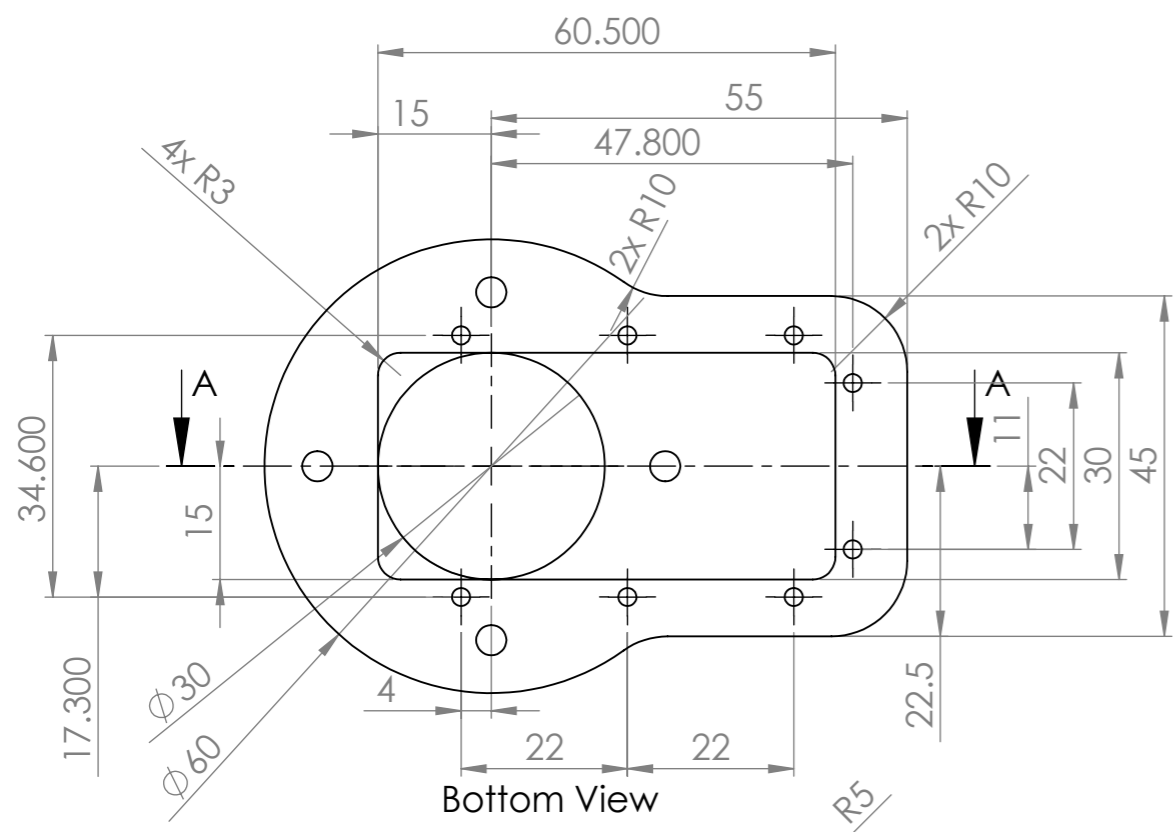
REVISION

NAME	SIGNATURE	DATE		
DRAWN				
CHK'D				
APPV'D				
MFG				
Q.A				

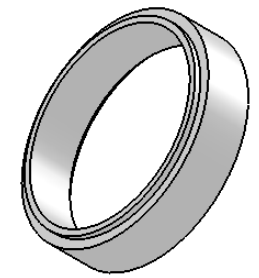
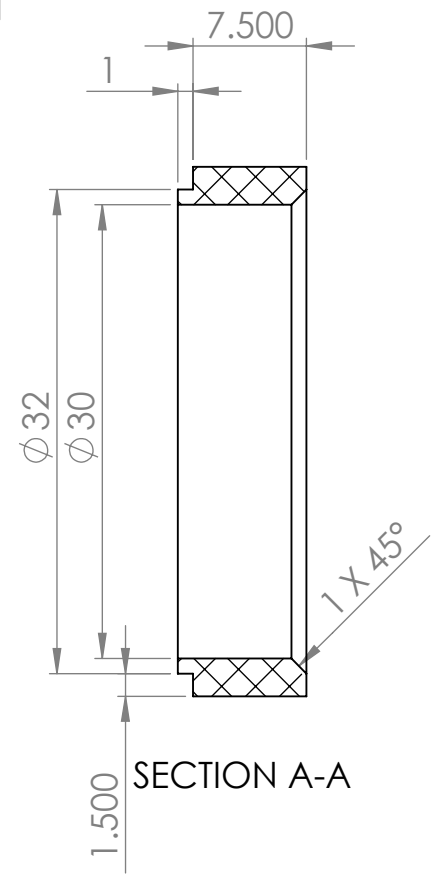
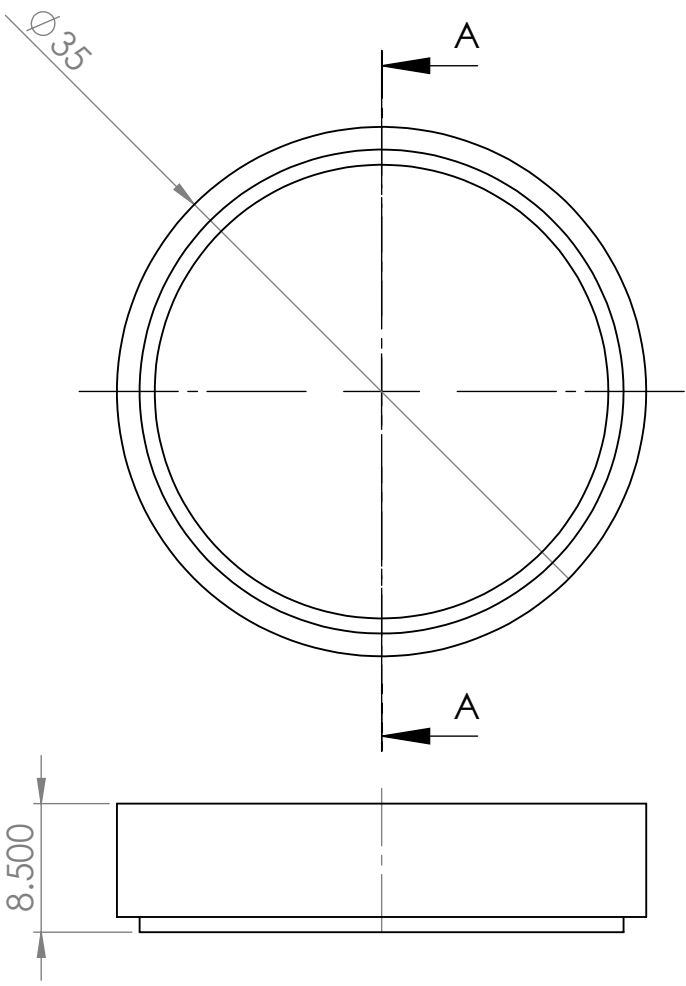
MATERIAL:
Aluminum 6061-T6

WEIGHT:

TITLE: <h1>Rudder Fixture</h1>	DWG NO. 3	A4
SCALE:1:1	SHEET 1 OF 1	



UNLESS OTHERWISE SPECIFIED: DIMENSIONS ARE IN MILLIMETERS SURFACE FINISH: TOLERANCES: LINEAR: ANGULAR:		FINISH:	DEBUR AND BREAK SHARP EDGES		DO NOT SCALE DRAWING	REVISION
NAME	SIGNATURE	DATE			TITLE: Motor Bracket	
DRAWN					DWG NO.	A4
CHK'D					4	
APPV'D					SCALE:1:1	
MFG						
Q.A			MATERIAL: Aluminum 6061-T6			
			WEIGHT:			SHEET 5 OF 25



UNLESS OTHERWISE SPECIFIED:
 DIMENSIONS ARE IN MILLIMETERS
 SURFACE FINISH:
 TOLERANCES:
 LINEAR:
 ANGULAR:

FINISH:

 DEBUR AND
 BREAK SHARP
 EDGES

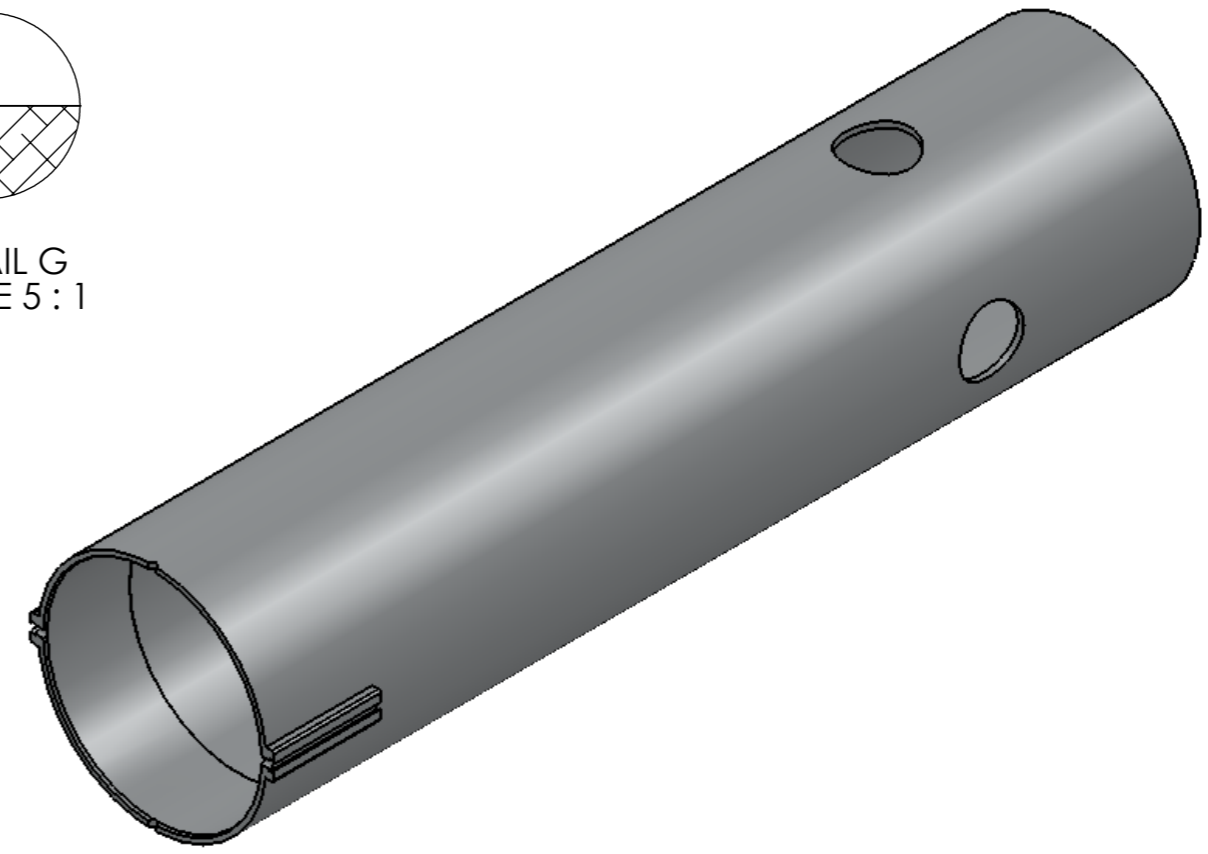
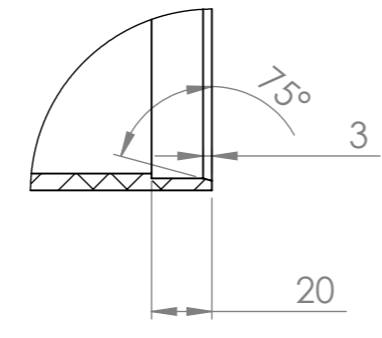
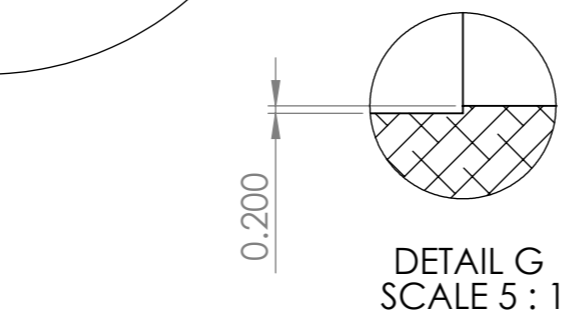
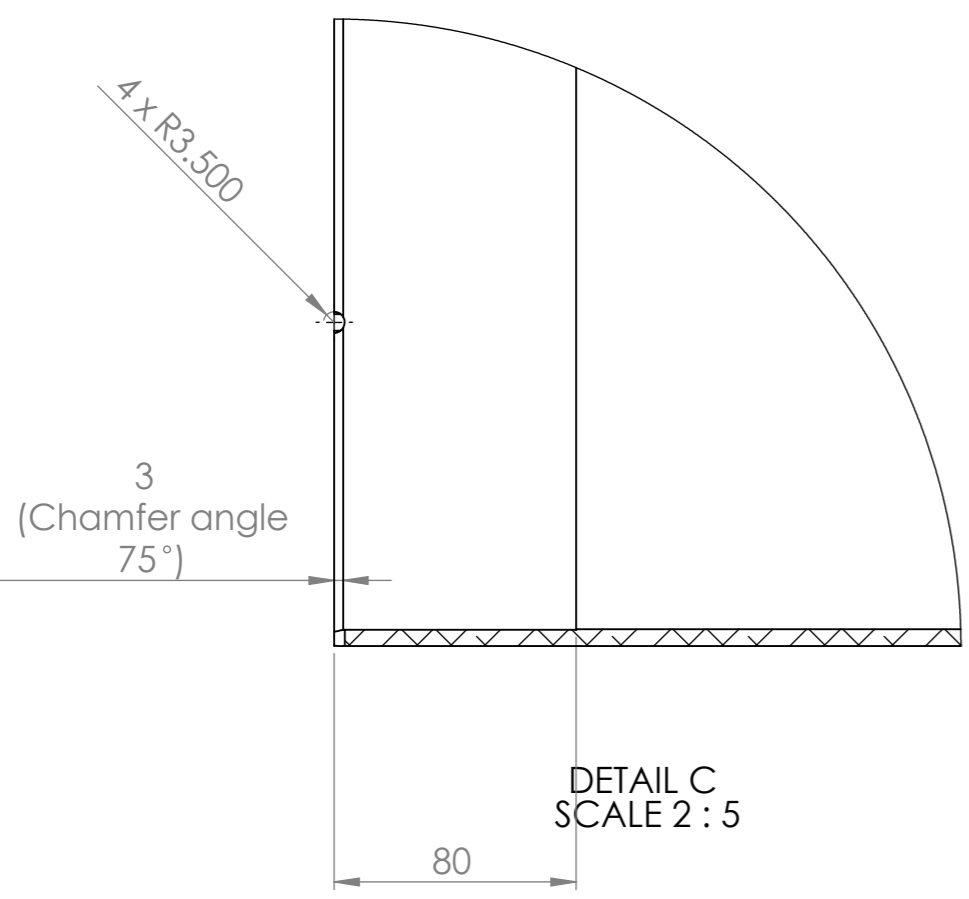
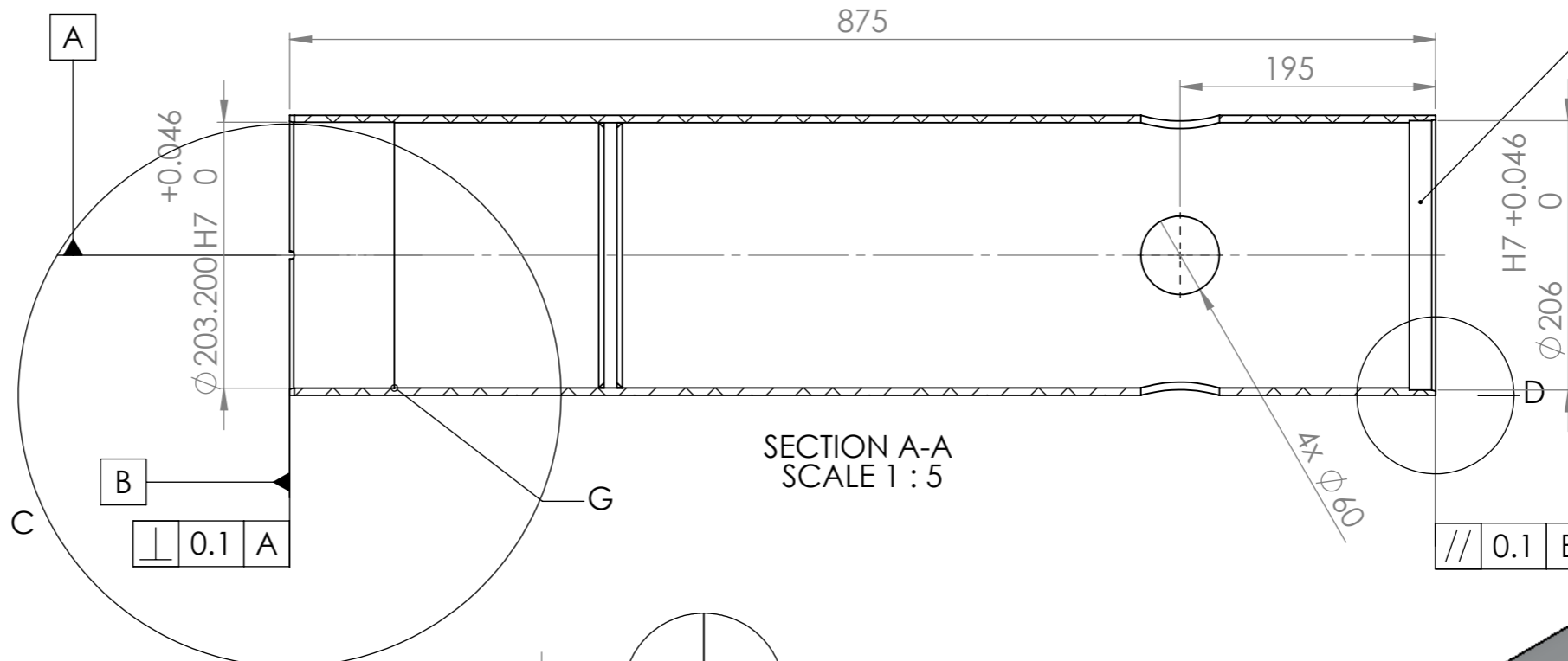
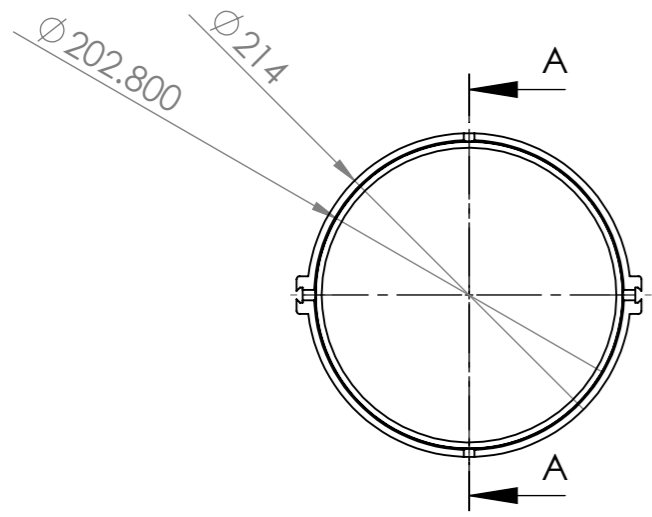
DO NOT SCALE DRAWING REVISION

	NAME	SIGNATURE	DATE		
DRAWN					
CHK'D					
APPV'D					
MFG					
Q.A					
				MATERIAL:	
				ABS Plastic	
				WEIGHT:	

TITLE:
Bearing Holding Ring

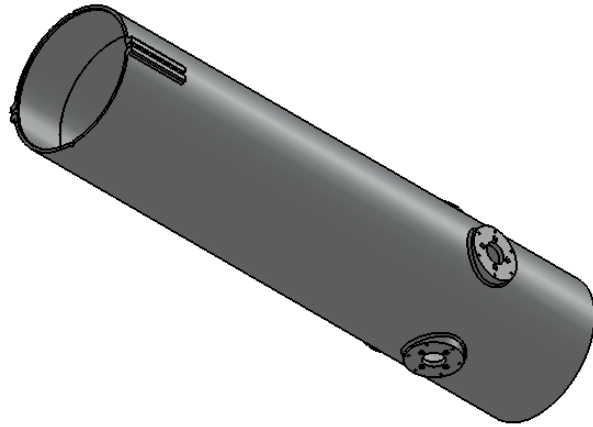
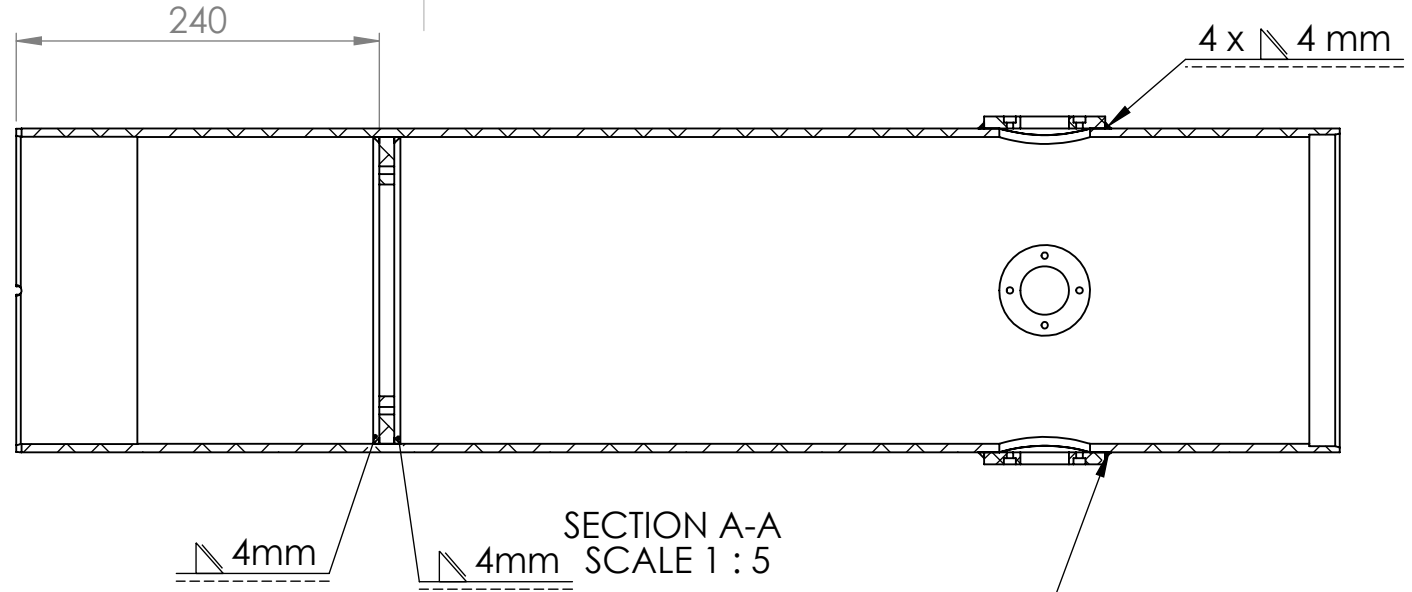
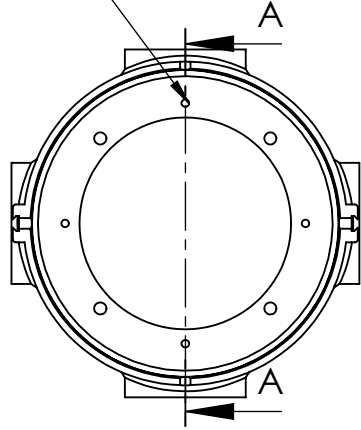
DWG NO. 5 A4

SCALE:2:1 SHEET 6 OF 25



UNLESS OTHERWISE SPECIFIED: DIMENSIONS ARE IN MILLIMETERS SURFACE FINISH: TOLERANCES: LINEAR: ANGULAR:				FINISH:	DEBUR AND BREAK SHARP EDGES	DO NOT SCALE DRAWING	REVISION
DRAWN	NAME	SIGNATURE	DATE			TITLE: <h1>Rear Cylinder</h1>	
CHK'D						DWG NO.	6
APPV'D						SCALE:1:5	SHEET 7 OF 25
MFG					MATERIAL: Aluminum 6061-T6		A4
Q.A					WEIGHT:		

Fixture Ring and Hole must be aligned



Rings must be welded all around and make sure they are leak-proof

UNLESS OTHERWISE SPECIFIED:
 DIMENSIONS ARE IN MILLIMETERS
 SURFACE FINISH:
 TOLERANCES:
 LINEAR:
 ANGULAR:

FINISH:

DEBUR AND
 BREAK SHARP
 EDGES

DO NOT SCALE DRAWING

REVISION

	NAME	SIGNATURE	DATE		
DRAWN					
CHK'D					
APPV'D					
MFG					
Q.A					
				MATERIAL:	
				Aluminum 6061-T6	
				WEIGHT:	

TITLE:

Rear Cylinder Welds

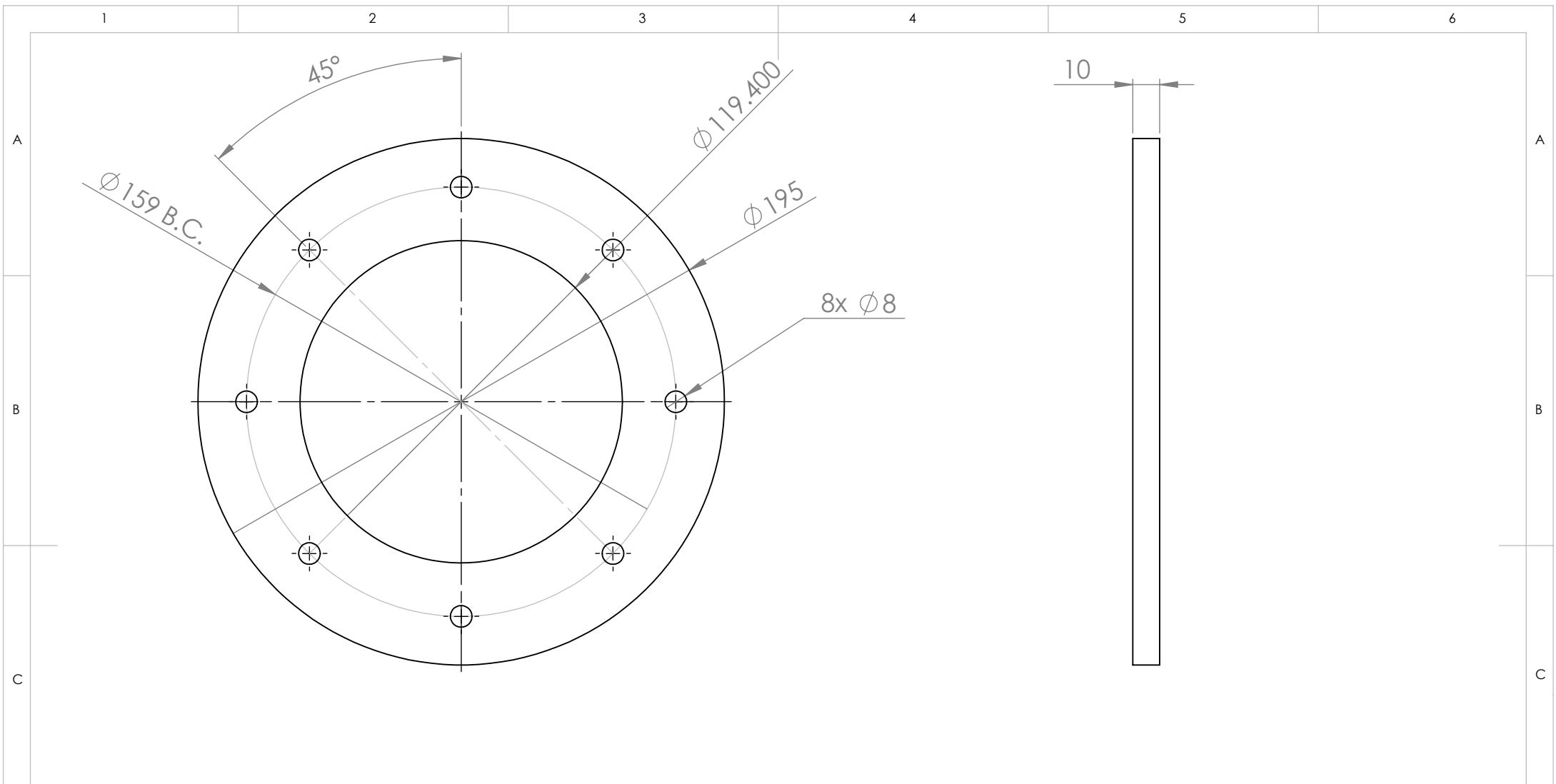
DWG NO.

7

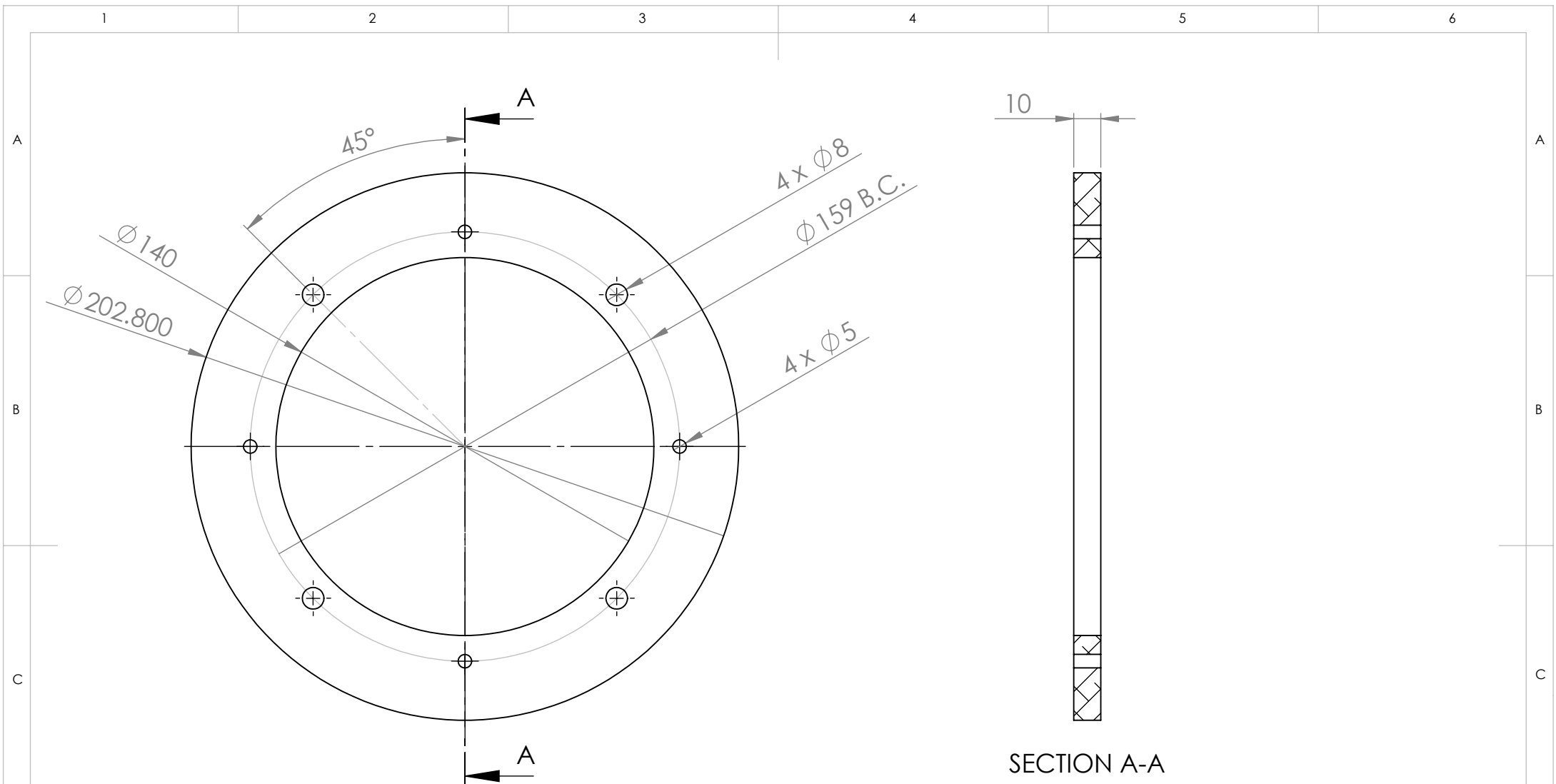
A4

SCALE:1:5

SHEET 8 OF 25

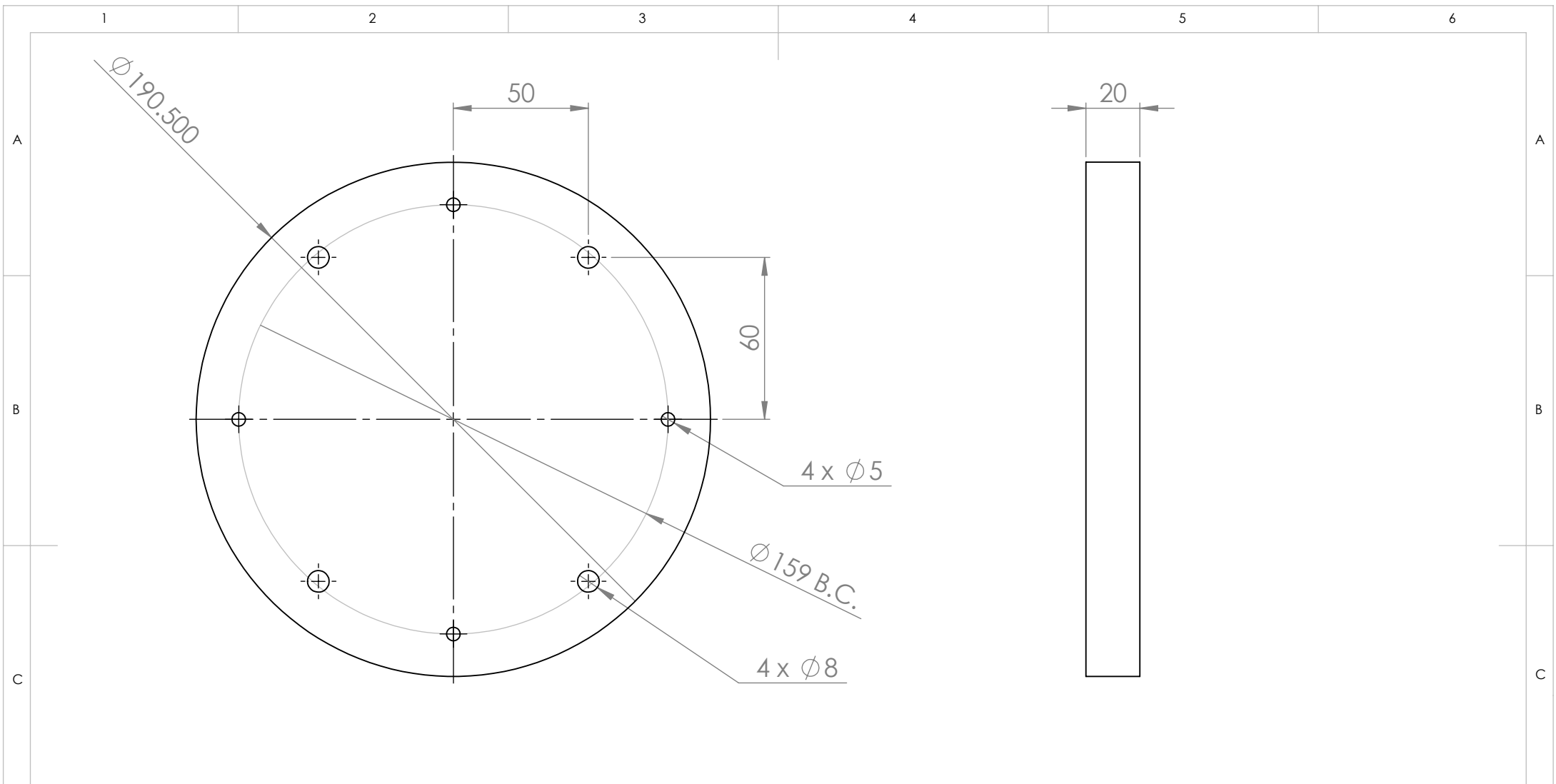


UNLESS OTHERWISE SPECIFIED: DIMENSIONS ARE IN MILLIMETERS				FINISH:		DEBUR AND BREAK SHARP EDGES		DO NOT SCALE DRAWING		REVISION	
SURFACE FINISH:											
TOLERANCES:											
LINEAR:											
ANGULAR:											
	NAME	SIGNATURE	DATE			TITLE:					
DRAWN						Propeller Connecting Plate					
CHK'D											
APPV'D											
MFG											
Q.A											
				MATERIAL:		DWG NO.		8		A4	
				Aluminum 6061-T6							
				WEIGHT:		SCALE:1:2		SHEET 9 OF 25			

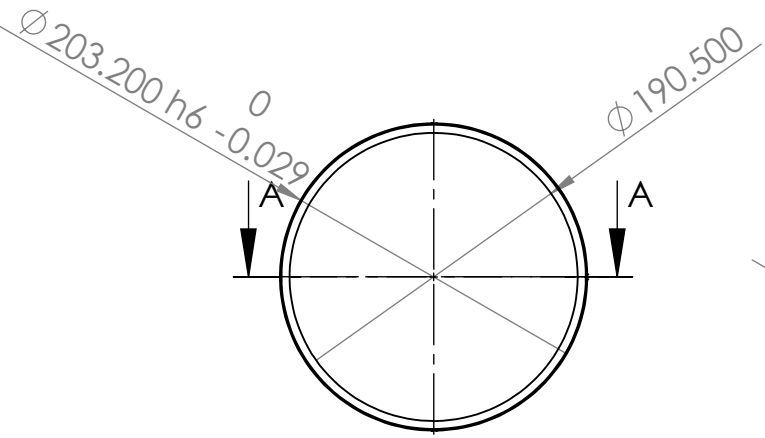


SECTION A-A

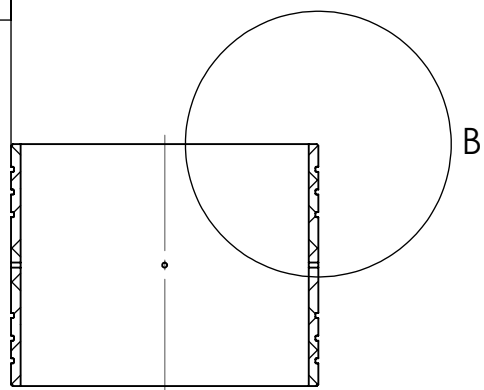
UNLESS OTHERWISE SPECIFIED: DIMENSIONS ARE IN MILLIMETERS		FINISH:		DEBUR AND BREAK SHARP EDGES		DO NOT SCALE DRAWING		REVISION	
SURFACE FINISH:									
TOLERANCES:									
LINEAR:									
ANGULAR:									
	NAME	SIGNATURE	DATE			TITLE:			
DRAWN						Rear Cylinder Connecting Plate			
CHK'D									
APPV'D									
MFG									
Q.A									
				MATERIAL: Aluminum 6061-T6		DWG NO. 9		A4	
				WEIGHT:		SCALE:1:2		SHEET 10 OF 25	



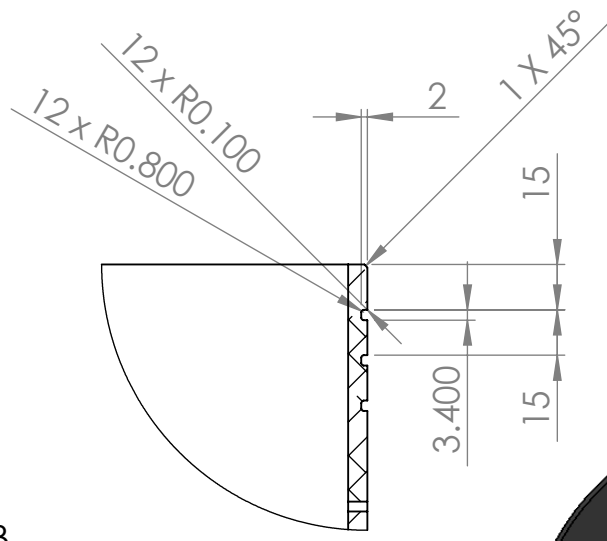
UNLESS OTHERWISE SPECIFIED: DIMENSIONS ARE IN MILLIMETERS SURFACE FINISH: TOLERANCES: LINEAR: ANGULAR:				FINISH:		DEBUR AND BREAK SHARP EDGES		DO NOT SCALE DRAWING		REVISION	
	NAME	SIGNATURE	DATE			TITLE: Middle adapter plate					
DRAWN						MATERIAL: Aluminum 6061-T6					
CHK'D											
APPV'D											
MFG											
Q.A						DWG NO.		10		A4	
						WEIGHT:		SCALE:1:2		SHEET 11 OF 25	



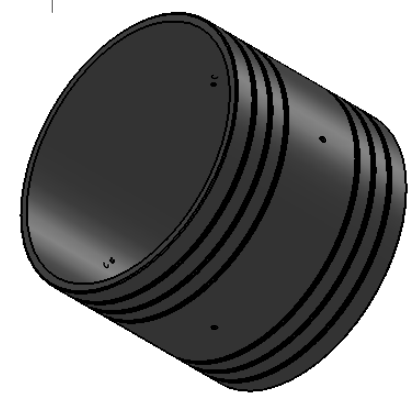
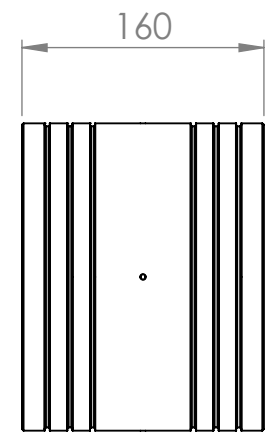
◎ 0.1 A



SECTION A-A



DETAIL B
SCALE 2 : 5



UNLESS OTHERWISE SPECIFIED:
 DIMENSIONS ARE IN MILLIMETERS
 SURFACE FINISH:
 TOLERANCES:
 LINEAR:
 ANGULAR:

FINISH:

 DEBUR AND
 BREAK SHARP
 EDGES

DO NOT SCALE DRAWING REVISION

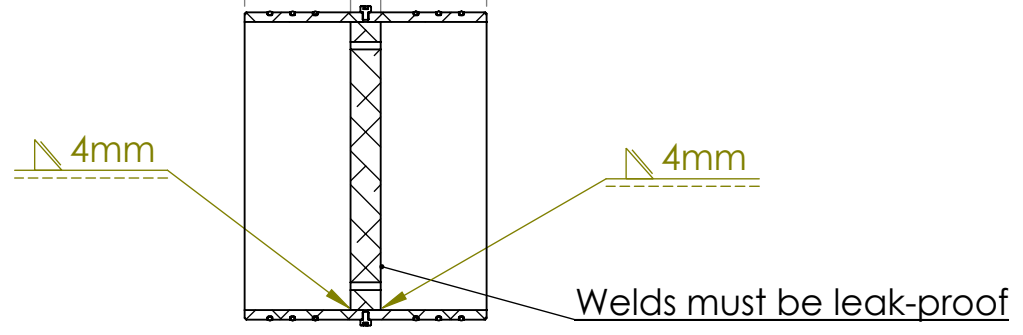
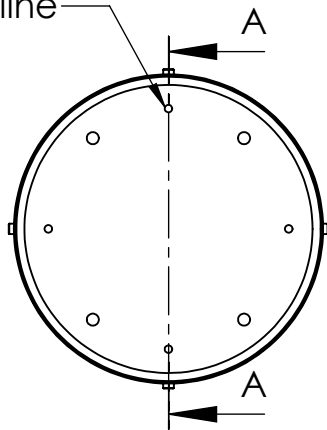
	NAME	SIGNATURE	DATE		
DRAWN					
CHK'D					
APPV'D					
MFG					
Q.A					

TITLE:
Middle Adapter

MATERIAL:
Aluminum 6061-T6

DWG NO. **11** **A4**

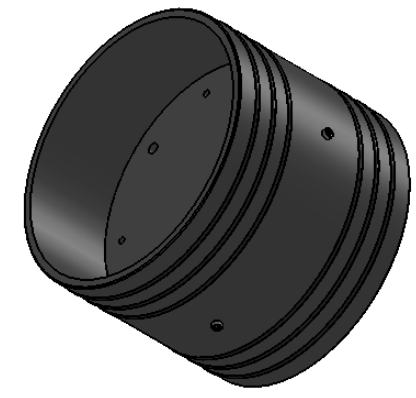
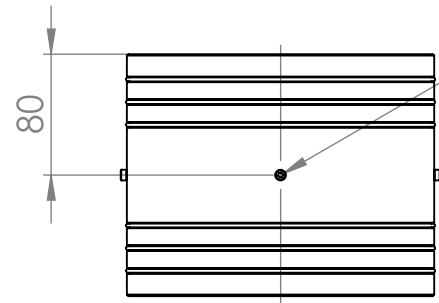
Holes must be aligned on the same line



SECTION A-A

4 x \varnothing 3.300 ∇ 7.100
M4x0.7 - 6H ∇ 5

Holes must be drilled after welding the plate



UNLESS OTHERWISE SPECIFIED:
DIMENSIONS ARE IN MILLIMETERS
SURFACE FINISH:
TOLERANCES:
LINEAR:
ANGULAR:

FINISH:

DEBUR AND
BREAK SHARP
EDGES

DO NOT SCALE DRAWING

REVISION

	NAME	SIGNATURE	DATE
DRAWN			
CHK'D			
APPV'D			
MFG			
Q.A			

TITLE:

Middle Adapter Welds

MATERIAL:
Aluminum 6061-T6

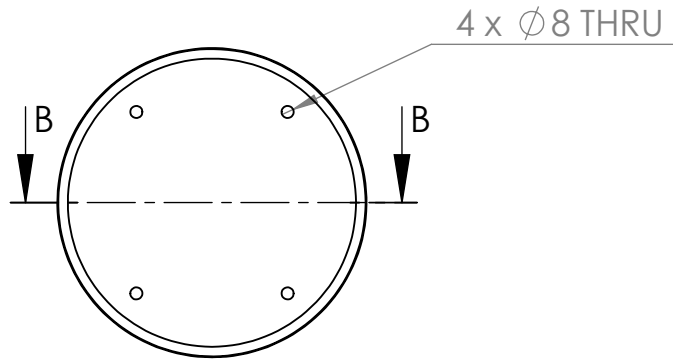
DWG NO. 12

A4

WEIGHT:

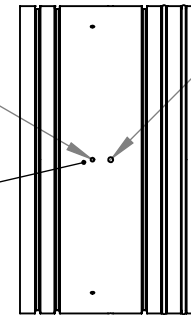
SCALE:1:5

SHEET 13 OF 25



6 x ϕ 2.500 ∇ 5.500
M3x0.5 - 6H ∇ 4

holes must be drilled
after welding the plate



4 x ϕ 3.300 ∇ 10.100
M4x0.7 - 6H ∇ 8

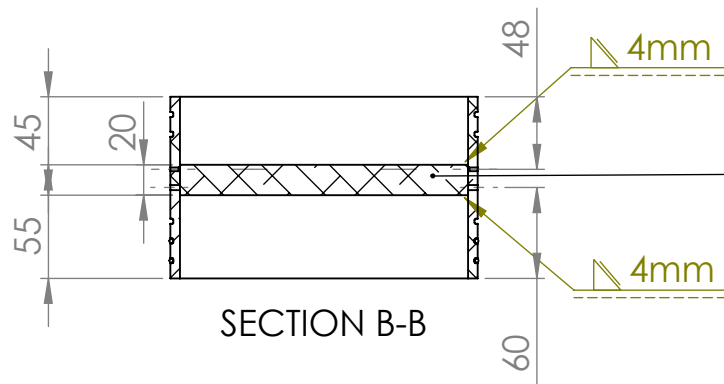


plate must be welded
all around and make sure
it is leak proof



UNLESS OTHERWISE SPECIFIED:
DIMENSIONS ARE IN MILLIMETERS
SURFACE FINISH:
TOLERANCES:
LINEAR:
ANGULAR:

FINISH:

DEBUR AND
BREAK SHARP
EDGES

DO NOT SCALE DRAWING

REVISION

	NAME	SIGNATURE	DATE		
DRAWN					
CHK'D					
APPV'D					
MFG					
Q.A					
				MATERIAL:	
				Aluminum 6061-T6	
				WEIGHT:	

TITLE:

Front Adapter

DWG NO.

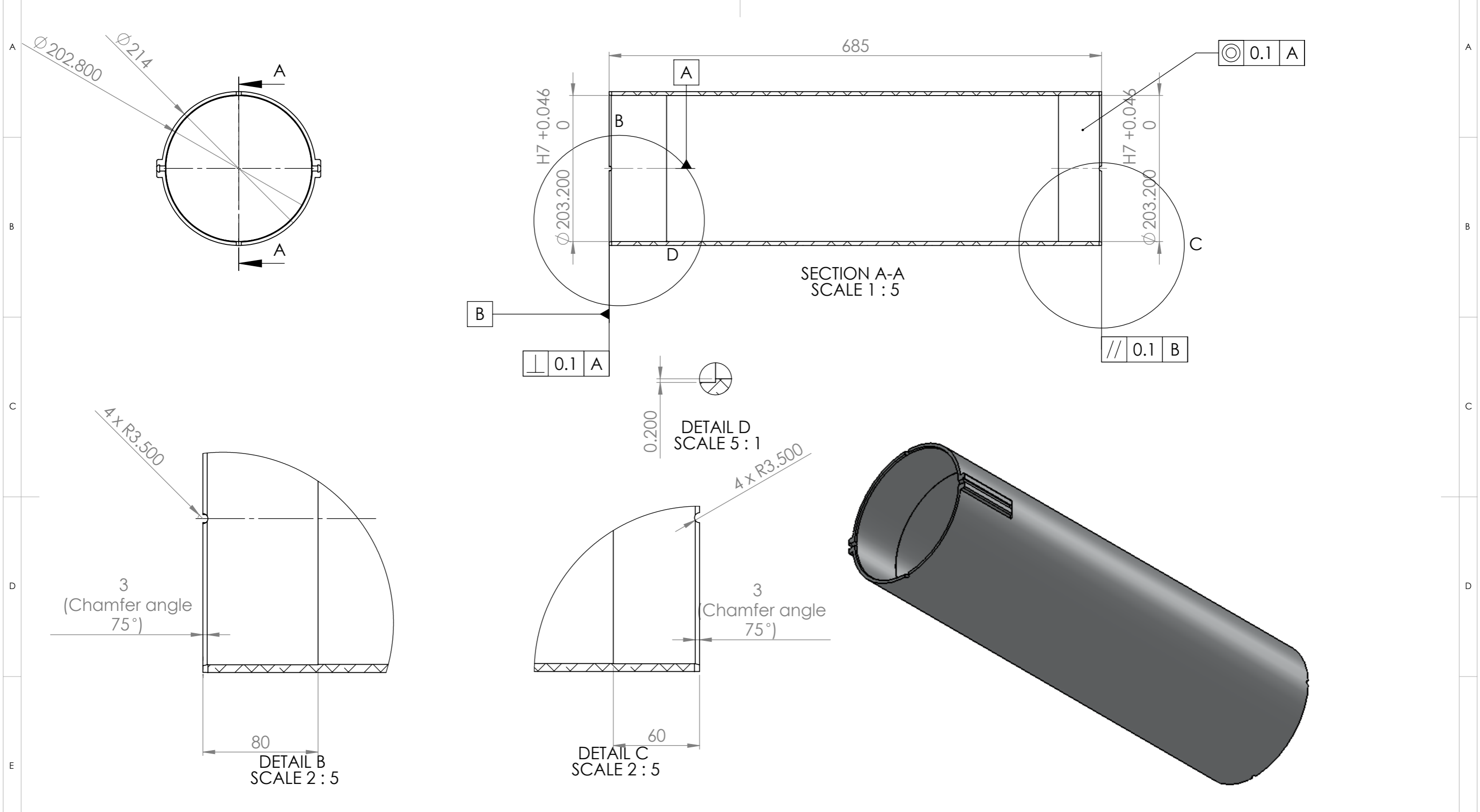
13

A4

SCALE:1:5

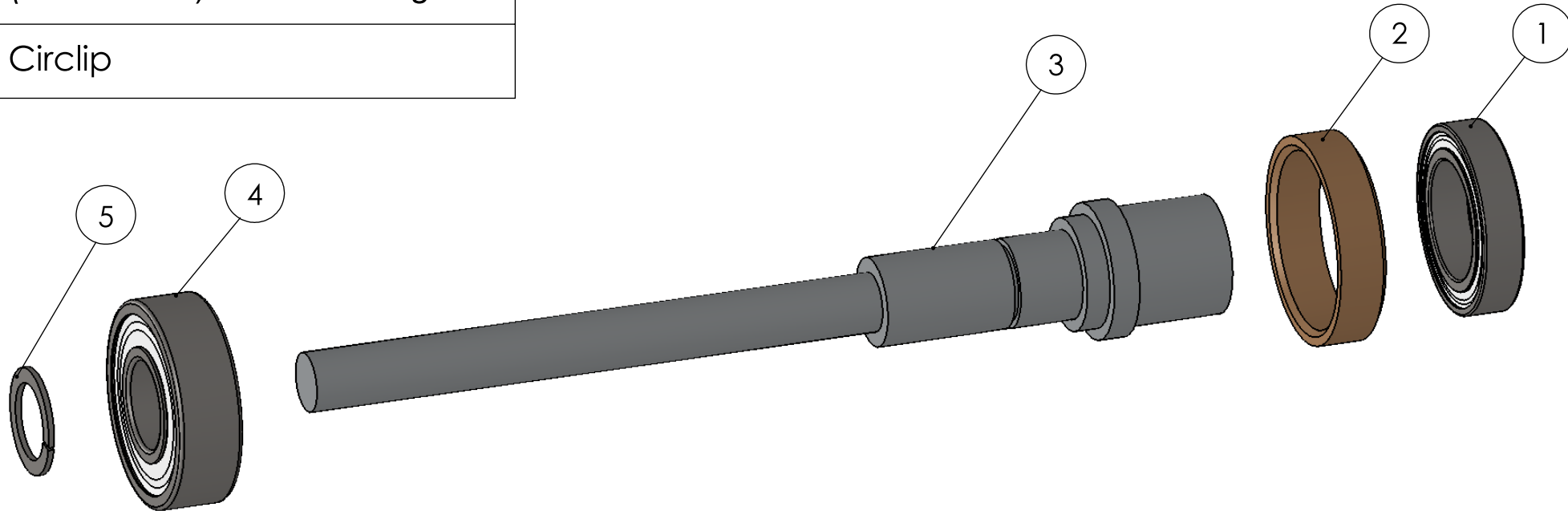
SHEET 16 OF 25

1 2 3 4 5 6 7 8



UNLESS OTHERWISE SPECIFIED: DIMENSIONS ARE IN MILLIMETERS SURFACE FINISH: TOLERANCES: LINEAR: ANGULAR:				FINISH:		DEBUR AND BREAK SHARP EDGES		DO NOT SCALE DRAWING		REVISION	
DRAWN				NAME		SIGNATURE		DATE		TITLE:	
CHK'D										Middle Cylinder	
APPV'D											
MFG										DWG NO.	
Q.A										14	
								MATERIAL:		A4	
								Aluminum 6061-T6		SCALE:1:1	
								WEIGHT:		SHEET 17 OF 25	

- | |
|------------------------------|
| 1. (61804-2RZ) SKF - Bearing |
| 2. Bearing Holding Ring |
| 3. Shaft |
| 5. (6202-2RSL) SKF - Bearing |
| 6. Circlip |



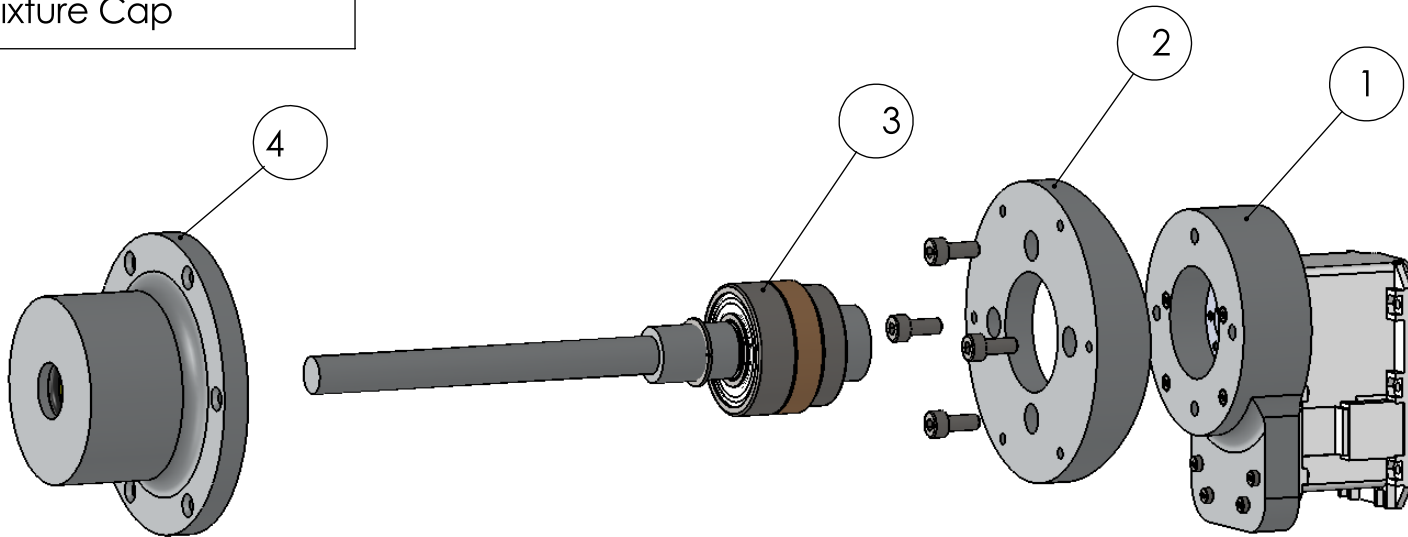
UNLESS OTHERWISE SPECIFIED: DIMENSIONS ARE IN MILLIMETERS SURFACE FINISH: TOLERANCES: LINEAR: ANGULAR:			FINISH:	DEBUR AND BREAK SHARP EDGES	DO NOT SCALE DRAWING	REVISION
	NAME	SIGNATURE	DATE		TITLE: Shaft Assembly	
DRAWN					DWG NO.	15
CHK'D					SCALE:1:1	SHEET 1 OF 1
APPV'D				MATERIAL:		A4
MFG				WEIGHT:		
Q.A						

1. Motor Bracket Assembly

2. Rudder Fixture Ring

3. Shaft and Bearing Assembly

4. Rudder Fixture Cap



UNLESS OTHERWISE SPECIFIED:
DIMENSIONS ARE IN MILLIMETERS
SURFACE FINISH:
TOLERANCES:
LINEAR:
ANGULAR:

FINISH:

DEBUR AND
BREAK SHARP
EDGES

DO NOT SCALE DRAWING

REVISION

	NAME	SIGNATURE	DATE				
DRAWN							
CHK'D							
APPV'D							
MFG							
Q.A							
					MATERIAL:		
					WEIGHT:		

TITLE:

Rudder Fixture Assembly

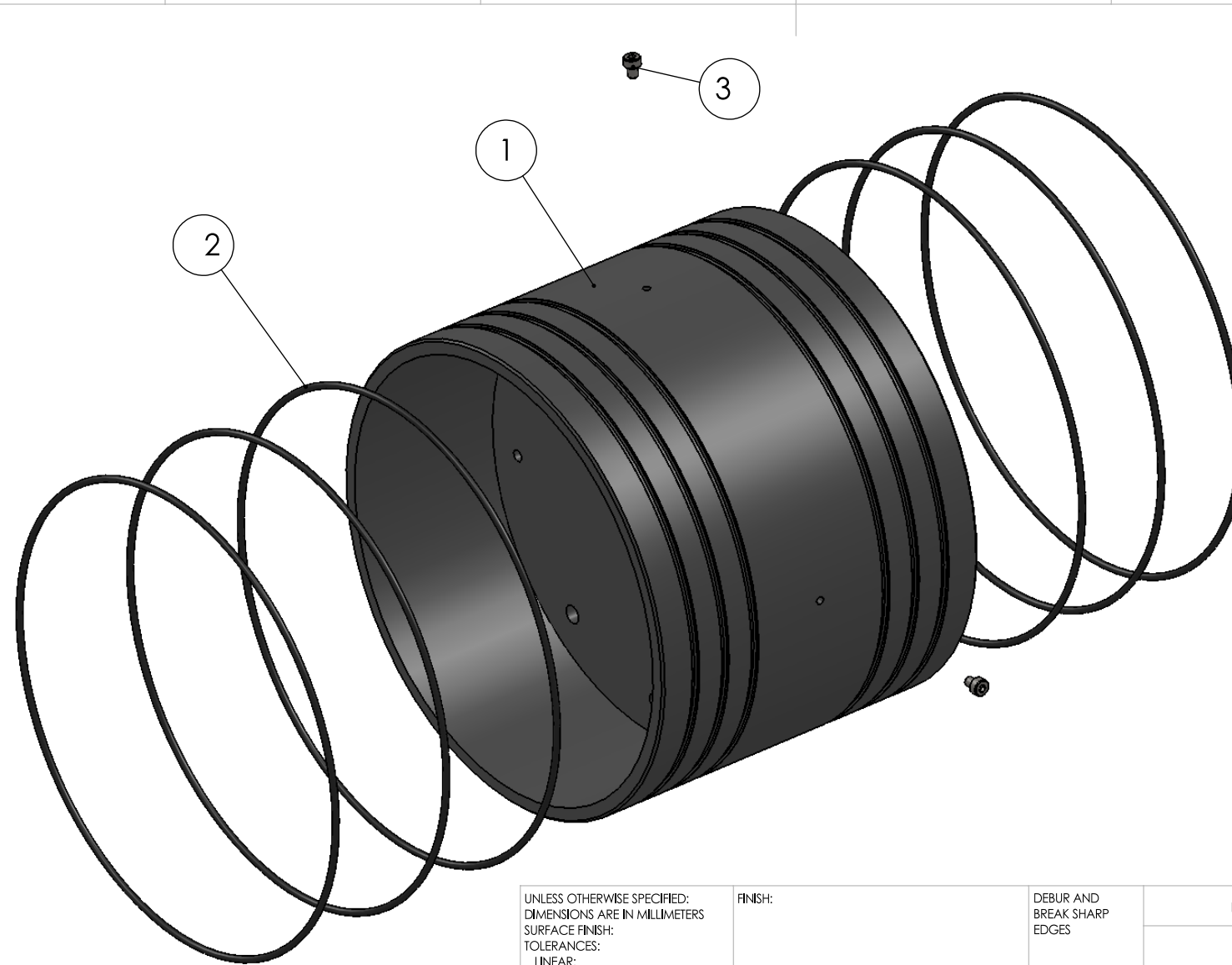
DWG NO.

16

A4

SCALE:1:1

SHEET 1 OF 1



- | |
|------------------------------|
| 1. Adapter |
| 2. O-ring 196.52x2.62 (x6) |
| 3. M4 Socket Head Screw (x4) |

UNLESS OTHERWISE SPECIFIED:
 DIMENSIONS ARE IN MILLIMETERS
 SURFACE FINISH:
 TOLERANCES:
 LINEAR:
 ANGULAR:
 FINISH:
 DEBUR AND BREAK SHARP EDGES

DO NOT SCALE DRAWING REVISION

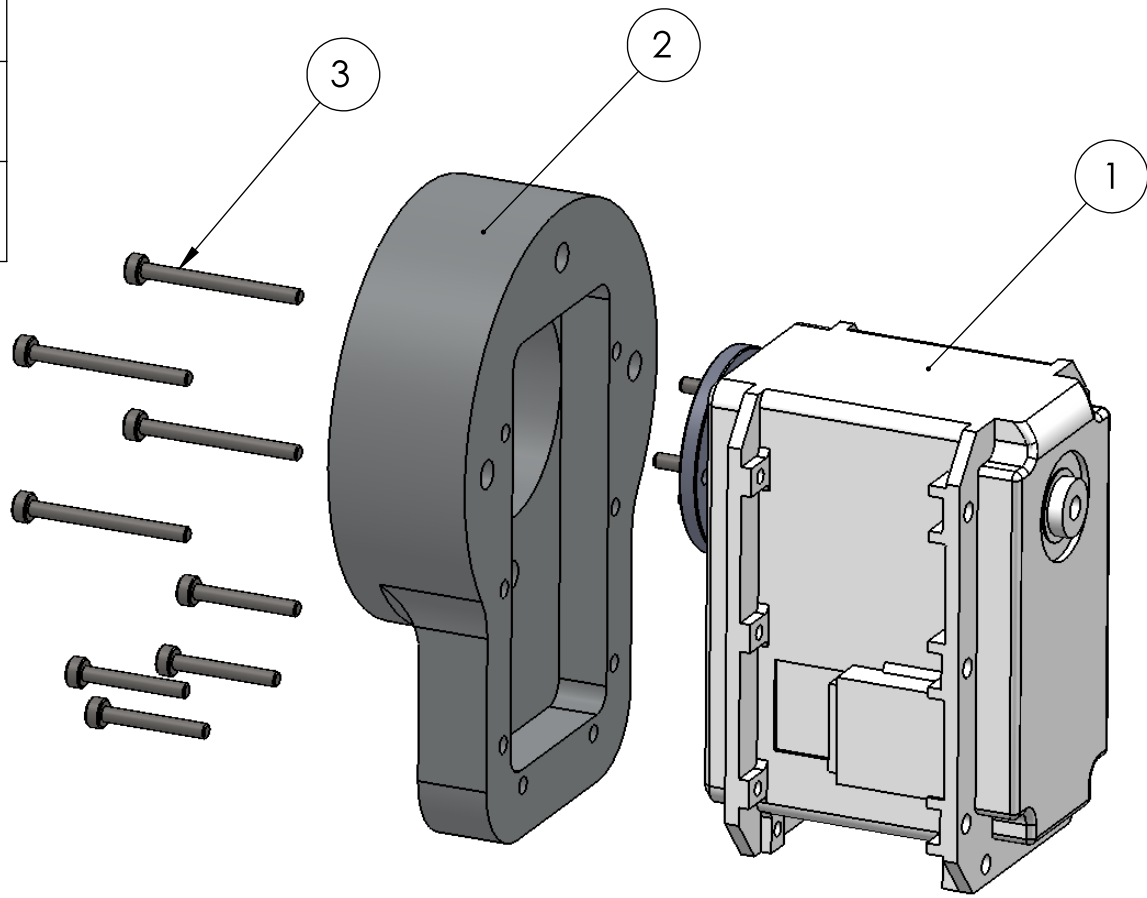
	NAME	SIGNATURE	DATE		
DRAWN					
CHK'D					
APPV'D					
MFG					
Q.A					

TITLE:
Middle Adapter Sub Assembly

MATERIAL:
 WEIGHT:

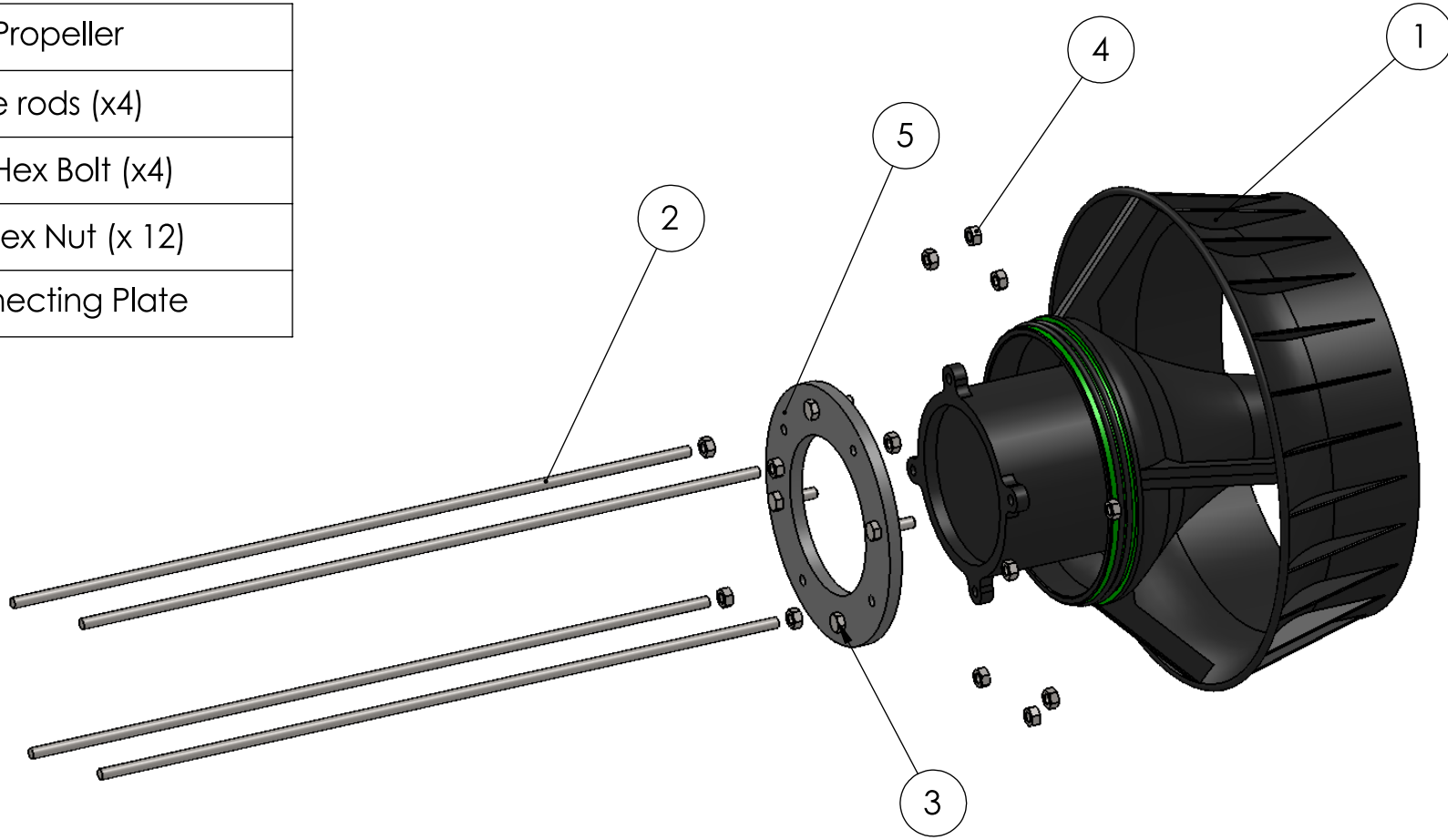
DWG NO. **17** A4

- 1. Dynamixel EX-106+
- 2. Motor Bracket
- 3. M2 Socket Head Screw



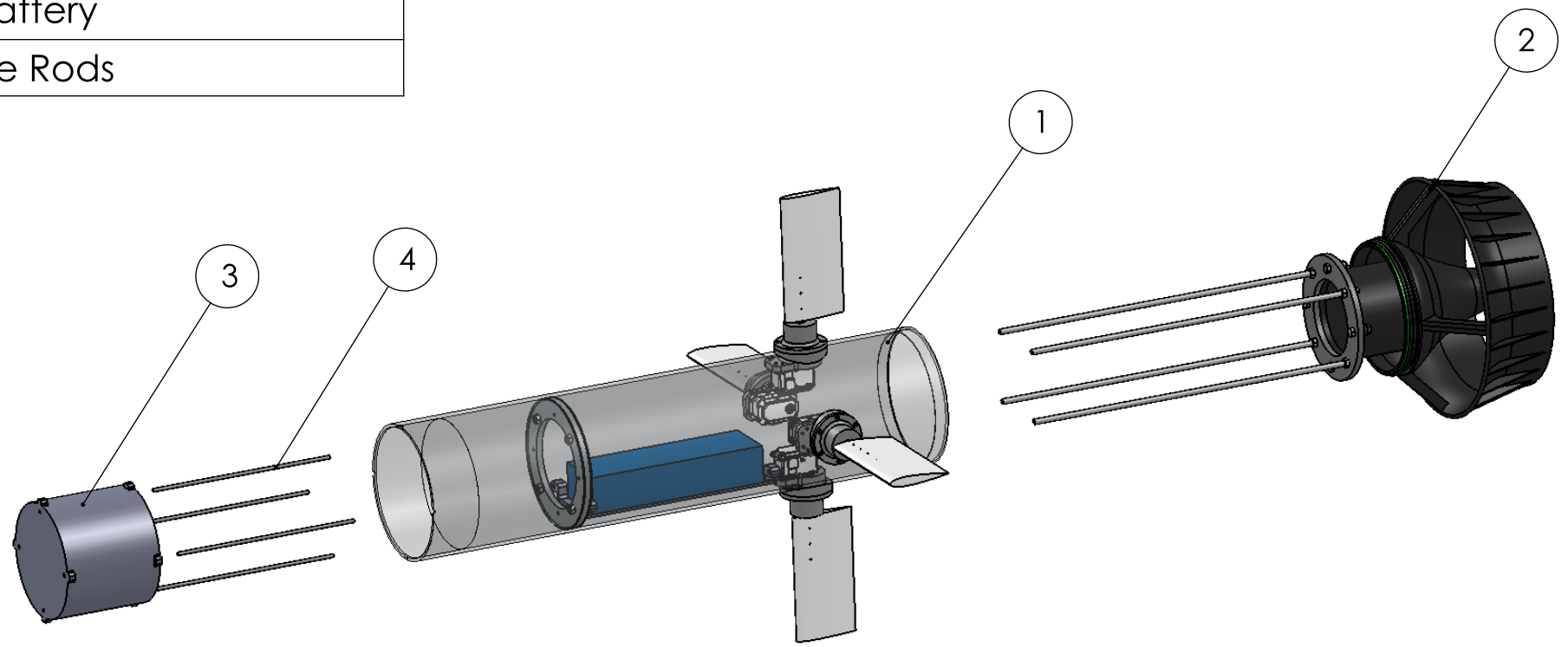
UNLESS OTHERWISE SPECIFIED: DIMENSIONS ARE IN MILLIMETERS SURFACE FINISH: TOLERANCES: LINEAR: ANGULAR:				FINISH:		DEBUR AND BREAK SHARP EDGES		DO NOT SCALE DRAWING		REVISION	
DRAWN	NAME	SIGNATURE	DATE					<h1 style="margin: 0;">Motor Bracket Assembly</h1>			
CHK'D											
APPV'D											
MFG											
Q.A											
				MATERIAL:		DWG NO.		18		A4	
				WEIGHT:		SCALE:1:1		SHEET 17 OF 25			

1. Propeller
2. Tie rods (x4)
3. M8 Hex Bolt (x4)
4. M8 Hex Nut (x 12)
5. Connecting Plate



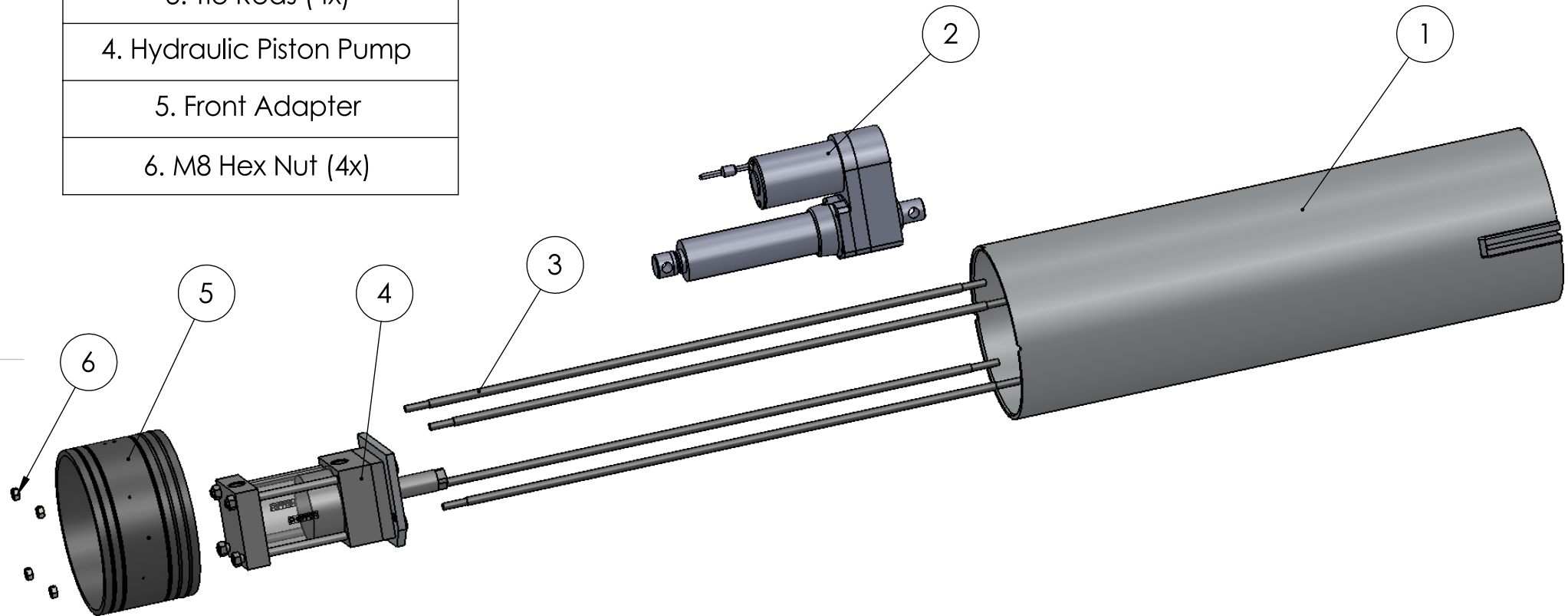
UNLESS OTHERWISE SPECIFIED: DIMENSIONS ARE IN MILLIMETERS SURFACE FINISH: TOLERANCES: LINEAR: ANGULAR:			FINISH:		DEBUR AND BREAK SHARP EDGES		DO NOT SCALE DRAWING		REVISION		
	NAME	SIGNATURE	DATE				TITLE: Propeller Sub Assembly				
DRAWN							DWG NO.		19		A4
CHK'D							SCALE:1:1		SHEET 21 OF 25		
APPVD							WEIGHT:				
MFG						MATERIAL:					
Q.A											

- | |
|--------------|
| 1. Rear Hull |
| 2. Propeller |
| 3. Battery |
| 4. Tie Rods |



UNLESS OTHERWISE SPECIFIED: DIMENSIONS ARE IN MILLIMETERS SURFACE FINISH: TOLERANCES: LINEAR: ANGULAR:		FINISH:	DEBUR AND BREAK SHARP EDGES		DO NOT SCALE DRAWING	REVISION
NAME	SIGNATURE	DATE	TITLE: <h1>Rear Assembly</h1>			
DRAWN			MATERIAL:	DWG NO.	20	A4
CHK'D				SCALE:1:1	SHEET 23 OF 25	
APPV'D			WEIGHT:			
MFG						
Q.A						

- 1. Middle Cylinder
- 2. Linear Actuator (SKF-CAHB20)
- 3. Tie Rods (4x)
- 4. Hydraulic Piston Pump
- 5. Front Adapter
- 6. M8 Hex Nut (4x)



UNLESS OTHERWISE SPECIFIED: DIMENSIONS ARE IN MILLIMETERS SURFACE FINISH: TOLERANCES: LINEAR: ANGULAR:			FINISH:		DEBUR AND BREAK SHARP EDGES		DO NOT SCALE DRAWING		REVISION		
	NAME	SIGNATURE	DATE				TITLE: <h2 style="margin: 0;">Front Assembly Exploded View</h2>				
DRAWN											
CHK'D											
APPV'D											
MFG											
Q.A					MATERIAL:		DWG NO.		21		A4
					WEIGHT:		SCALE:		SHEET 24 OF 25		

1 2 3 4 5 6

A

B

C

D

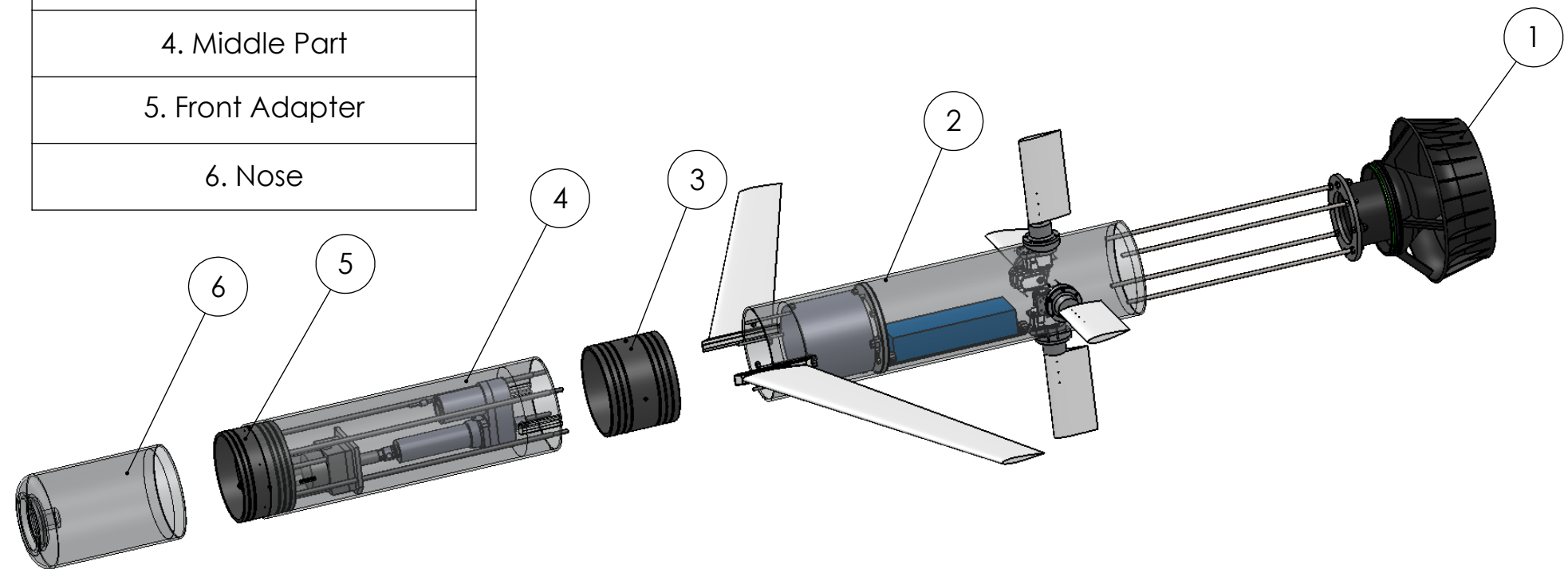
A

B

C

D

- | |
|-------------------|
| 1. Propeller |
| 2. Rear Part |
| 3. Middle Adapter |
| 4. Middle Part |
| 5. Front Adapter |
| 6. Nose |



UNLESS OTHERWISE SPECIFIED:
 DIMENSIONS ARE IN MILLIMETERS
 SURFACE FINISH:
 TOLERANCES:
 LINEAR:
 ANGULAR:
 FINISH:
 DEBUR AND
 BREAK SHARP
 EDGES

DO NOT SCALE DRAWING REVISION

	NAME	SIGNATURE	DATE		
DRAWN					
CHK'D					
APPV'D					
MFG					
Q.A					
				MATERIAL:	
				WEIGHT:	

TITLE:
Full Assembly Exploded View
 DWG NO. **22** A4

1 2 3 4 5 6

SCALE: SHEET 25 OF 25